PERMEABILITY TESTING OF SHEARING

FRACTURES IN ROCK

Jiranut Obcheoy

A Thesis Submitted in Partial Fulfillment of the Requirements for the

Degree of Master of Engineering in Geotechnology

Suranaree University of Technology

Academic Year 2010

การทดสอบความซึมผ่านของรอยแตกในหินภายใต้แรงเฉือน

นางสาวจิรานัท อบเชย

วิทยานิพนธ์นี้เป็นส่วนหนึ่งของการศึกษาตามหลักสูตรปริญญาวิศวกรรมศาสตรมหาบัณฑิต
สาขาวิชาเทคโนโลยีธรณี
มหาวิทยาลัยเทคโนโลยีสุรนารี
ปีการศึกษา 2553

PERMEABILITY TESTING OF SHEARING

FRACTURES IN ROCK

Suranaree University of Technology has approved this thesis submitted in partial fulfillment of the requirements for the Master's degree.

Thesis Examining Committee

_____

(Asst. Prof. Thara Lekuthai)

Chairperson

_____

(Assoc. Prof. Dr. Kittitep Fuenkajorn)

Member (Thesis Advisor)

_____

(Dr. Prachya Tepnarong)

Member

_____   _____

(Dr. Wut Dankittikul)   (Assoc. Prof. Dr. Vorapot Khompis)

Acting Vice Rector for Academic Affairs   Dean of Institute of Engineering

จิรานัท อบเชย : การทดสอบความซึมผ่านของรอยแตกในหินภายใต้แรงเฉือน
(PERMEABILITY TESTING OF SHEARING FRACTURES IN ROCK)
อาจารย์ที่ปรึกษา : รองศาสตราจารย์ ดร.กิตติเทพ เฟื่องขจร, 69 หน้า.

วัตถุประสงค์ของงานวิจัยนี้คือเพื่อศึกษาค่าสัมประสิทธิ์ความซึมผ่านของรอยแตกในหิน
ภายใต้ความเค้นตั้งฉากและความเค้นเฉือน โดยใช้การทดสอบการไหลของน้ำด้วยวิธีอัดน้ำด้วย
แรงดันแบบผันแปรบนรอยแตกที่ทำขึ้นในห้องปฏิบัติการ ตัวอย่าง 4 ชนิด ได้แก่ หินอ่อน
จากจังหวัดสระบุรี หินแกรนิตจากจังหวัดตาก หินแกรนิตจากประเทศจีนและหินแกรนิต
จากประเทศเวียดนาม พื้นที่ผิวรอยแตกมีขนาดเท่ากับ 10×10 ตารางเซนติเมตร มีการเจาะรูตรงกลาง
ของตัวอย่างหินชิ้นล่างเพื่อให้การไหลของน้ำผ่านรอยแตก ให้แรงเฉือนบนตัวอย่างหินขณะที่มี
การตรวจวัดการไหลเข้า ค่าความเค้นตั้งฉากบนรอยแตกผันแปรตั้งแต่ 1 ถึง 4 เมกะปาสคาล ผลที่ได้
ระบุว่าการเปิดเผยเชิงกายภาพ (e_p) และเชิงไฮดรอลิค (e_h) จะเพิ่มขึ้นตามการเคลื่อนตัวแบบเฉือน
ซึ่งจะเห็นได้ชัดสำหรับรอยแตกภายใต้ความเค้นตั้งฉากที่มีค่าสูง ความซึมผ่านของรอยแตกภายใต้
สภาวะที่ไม่มีแรงเฉือนและสภาวะที่มีแรงเฉือนสูงสุดจะมีค่าใกล้เคียงกัน การเปิดเผยเชิงกายภาพ
จะมีค่ามากกว่าการเปิดเผยเชิงไฮดรอลิคประมาณ 5 ถึง 10 เท่า ส่งผลให้ค่าสัมประสิทธิ์
ความซึมผ่านเชิงกายภาพสูงกว่าค่าความซึมผ่านเชิงไฮดรอลิค เนื่องจากว่าการเปิดเผยเชิงกายภาพ
ไม่พิจารณผลกระทบของความขรุขระของรอยแตกที่เป็นปัจจัยทำให้ระยะทางของการไหลของน้ำ
ยาวขึ้น ผลต่างระหว่างค่าความซึมผ่านภายใต้ความเค้นสูงสุดและภายใต้ความเค้นคงเหลือจะมีค่า
มากขึ้นเมื่อความเค้นตั้งฉากบนรอยแตกนั้นมีค่ามากขึ้น ค่าสัมประสิทธิ์ความซึมผ่านของรอยแตก
จะมีค่าลดลงเมื่อความเค้นตั้งฉากมีค่าสูงขึ้น ค่าความซึมผ่านที่ได้จากงานวิจัยนี้มีค่าระหว่าง $1×10^{-3}$
เมตร/วินาที ถึง $15×10^{-3}$ เมตร/วินาที เพื่อแสดงผลกระทบของการเคลื่อนตัวของรอยแตกได้ทำการ
วิเคราะห์โดยใช้โปรแกรม UDEC โดยจำลองการเคลื่อนตัวของรอยแตกในมวลหินบนอุโมงค์
รูปสี่เหลี่ยมผืนผ้า ผลจากการจำลองก่อนการขุดเจาะพบว่าค่าความซึมผ่านของรอยแตกจะลดลงเมื่อ
ความลึกมากขึ้น หลังการขุดเจาะอุโมงค์พบว่ามีการเคลื่อนตัวของรอยแตกมากขึ้นที่บริเวณขอบ
อุโมงค์ ซึ่งส่งผลให้มีค่าความซึมผ่านของรอยแตกมากขึ้น ความเค้นและการเคลื่อนตัวของรอยแตก
ที่ได้จากการจำลองสามารถนำมาประยุกต์ใช้หาค่าสัมประสิทธิ์ความซึมผ่านทั้งก่อนและหลังการ
ขุดเจาะในมวลหินอื่น ๆ ได้

สาขาวิชาเทคโนโลยีธรณี   ลายมือชื่อนักศึกษา _____
ปีการศึกษา 2553   ลายมือชื่ออาจารย์ที่ปรึกษา _____

JIRANUT OBCHEOY : PERMEABILITY TESTING OF SHEARING

FRACTURES IN ROCK. THESIS ADVISOR : ASSOC. PROF. KITTITEP

FUENKAJORN, Ph.D., P.E., 69 PP.

FRACTURE/PERMEABILITY/APERTURE/SHEAR STRESS

The objectives of this research are to experimentally determine hydraulic conductivity of tension-induced fractures under normal and shear stresses. The effort primarily involves performing a series falling head tests on tension-induced fractures. The fractures in four types of rock samples include Saraburi marble, Tak granite, Vietnamese granite and Chinese granite. The tested fracture area is 10×10 square centimeters. A small center hole is drilled into the lower block of the sample to allow water flow through the fracture. The shear force is applied while the flow rates are monitored. The constant normal stresses on the fracture are varied from 1 to 4 MPa. The results indicate that the physical aperture (e_p) and hydraulic aperture (e_h) increase with shearing displacement, particularly under high normal stresses. The magnitudes of fracture permeability under no shear and under peak shear stress are similar. For both peak and residual regions, the physical apertures are about 5 to 10 times greater than the hydraulic apertures, as a result the fracture hydraulic conductivity determined from the physical aperture are about one to two orders of magnitudes greater than those determined from the equivalent hydraulic apertures. This is probably because the measured physical apertures do not consider the effect of fracture roughness that causes a longer flow path. The difference between the permeability under residual shear stress and that under peak stress becomes larger under higher normal stresses. The fracture hydraulic conductivities exponentially decrease with increasing normal

stresses. Their permeability is in the range between 1×10^{-3} m/s and 15×10^{-3} m/s. To demonstrate these issues discrete element analyses are performed using UDEC to simulate the movement of the jointed rock mass above a rectangular underground excavation. Simulation results before excavation show that the joint permeability decreases when the depth increases. Under the excavated condition, the joint movement occurs around the zone of excavation, and results in an increase of the rock joint permeability. The stress and joint displacement can be used to determine the hydraulic conductivity obtains before and after excavation.

School of <u>Geotechnology</u>   Student's Signature _____

Academic Year 2010   Advisor's Signature_____

ACKNOWLEDGEMENTS

TABLE OF CONTENTS

TABLE OF CONTENTS (Continued)

Page

LIST OF TABLES

Table **Page**

LIST OF FIGURES

Figure   **Page**

LIST OF FIGURES (Continued)

LIST OF FIGURES (Continued)

LIST OF FIGURES (Continued)

LIST OF SYMBOLS AND ABBREVIATIONS

A_0 =   Empirical constant depend on the normal stresses for equation (4.8)

B_0 =   Empirical constant depend on the normal stresses for equation (4.8)

c   =   Cohesion

e_h =   Hydraulic aperture

e_m =   Mechanical aperture

e_p =   Physical aperture

H_1, H_2 =   Excess pressure head at beginning and end of test

JCS   =   Joint compressive strength

JRC   =   Joint roughness coefficient

K   =   Hydraulic conductivity

K_h =   Hydraulic conductivity (determined from hydraulic aperture)

K_m =   Hydraulic conductivity (determined from mechanical aperture)

K_p =   Hydraulic conductivity (determined from physical aperture)

k_n =   Joint normal stiffness

k_s =   Joint shear stiffness

R   =   Radius of flow path

R^2 =   Coefficient of determination

r   =   Radius of injection hole

r_b =   Pipette radius

t_1, t_2 =   Time at beginning and end of test

LIST OF SYMBOLS AND ABBREVIATIONS (Continued)

α_p	=	Empirical constant for equation (4.6)
α_r	=	Empirical constant for equation (4.7)
β_p	=	Empirical constant for equation (4.6)
β_r	=	Empirical constant for equation (4.7)
δ_n	=	Normal displacement
δ_s	=	Shear displacement
ϕ_p	=	Peak friction angle
ϕ_r	=	Residual friction angle
γ	=	Unit weight of water
μ	=	Dynamic viscosity
σ_c	=	Uniaxial compressive strength
σ_n	=	Normal stress
τ	=	Shear stress
τ_p	=	Peak shear strength
τ_r	=	Residual shear strength

CHAPTER I

INTRODUCTION

1.1 Background of problems and significance of the study

Groundwater in rock mass is one of the key factors governing the mechanical stability of slope embankments, underground mines and tunnels. Permeability of rock mass is path dependent, controlling mainly by the system of fractures as the permeability of most intact rocks is significantly lower. For undisturbed rock mass (before excavation) the joint characteristics that dictate the amount and direction of water flow, can be adequately determined by means of in-situ measurements, and sometimes assisted by numerical modeling. Slope or underground excavations disturb the surrounding rock mass, alter the stress states on the fracture planes, and often cause relative displacements of the fractures. The excavations usually increase the surrounding rock mass permeability, sometimes by several orders of magnitudes. Even though this effect has long been recognized, study on the rock fracture permeability as affected by the shearing displacement has been rare.

1.2 Research objectives

The objective of this research is to experimentally assess the permeability of rock fractures under shearing displacements. The effort primarily involves performing a series falling head tests on tension-induced fractures in four samples, including Saraburi marble, Tak granite, Vietnamese granite and Chinese granite. The changes

of the physical and hydraulic apertures, the water flow rates, and the applied shear stresses are monitored and used to calculate the changes of the fracture permeability as a function of shear displacement. The finite difference analysis (UDEC) is performed to determine the permeability increase zone induced by excavations in rock mass.

1.3   Research methodology

As shown in Figure 1.1, the research methodology comprises 7 steps; including literature review, sample preparation, flow testing, determination of the joint normal and shear stiffness (k_n, k_s), frictions angle (ϕ), cohesion (c) and hydraulic conductivity (K), development of mathematical relations, numerical analysis, conclusions and thesis writing.

1.3.1   Literature review

Literature review is carried out to study the genesis and classification of fractures, permeability of rock mass, apertures, and stress effects on fracture void geometry. The sources of information are from text books, journals, technical reports and conference papers. A summary of the literature review is given in the thesis.

1.3.2   Sample collection and preparation

Sample preparation is carried out in the laboratory at the Suranaree University of Technology. Samples for the falling head test are prepared to have fractures area of about 10×10 cm^2. The fractures are artificially made in the laboratory by tension inducing method.

```
┌─────────────────────────────────────────────────────────────┐
│                                                             │
│                    ┌──────────────────────┐                 │
│                    │   Literature Review   │                 │
│                    └──────────────────────┘                 │
│                               │                             │
│                               ▼                             │
│                    ┌──────────────────────┐                 │
│                    │  Sample Preparation   │                 │
│                    └──────────────────────┘                 │
│                               │                             │
│                               ▼                             │
│                  ┌──────────────────────────┐               │
│                  │   Falling Head Flow Tests │               │
│                  │   under Direct Shear Tests│               │
│                  └──────────────────────────┘               │
│                               │                             │
│                               ▼                             │
│                  ┌──────────────────────────┐               │
│                  │ Determination of ks, kn,  │               │
│                  │        φ, c and K         │               │
│                  └──────────────────────────┘               │
│                               │                             │
│                               ▼                             │
│                 ┌────────────────────────────┐              │
│                 │ Development of Mathematical │              │
│                 │ Relations between K and σn, δs│            │
│                 └────────────────────────────┘              │
│                               │                             │
│                               ▼                             │
│                  ┌──────────────────────────┐               │
│                  │   Numerical Analysis      │               │
│                  │        (UDEC)             │               │
│                  └──────────────────────────┘               │
│                               │                             │
│                               ▼                             │
│                ┌──────────────────────────────┐             │
│                │ Conclusions and Thesis Writing│             │
│                └──────────────────────────────┘             │
│                                                             │
└─────────────────────────────────────────────────────────────┘
```

Boxes in the flowchart (top to bottom):

- Literature Review
- Sample Preparation
- Falling Head Flow Tests under Direct Shear Tests
- Determination of k_s, k_n, ϕ, c and K
- Development of Mathematical Relations between K and σ_n, δ_s
- Numerical Analysis (UDEC)
- Conclusions and Thesis Writing
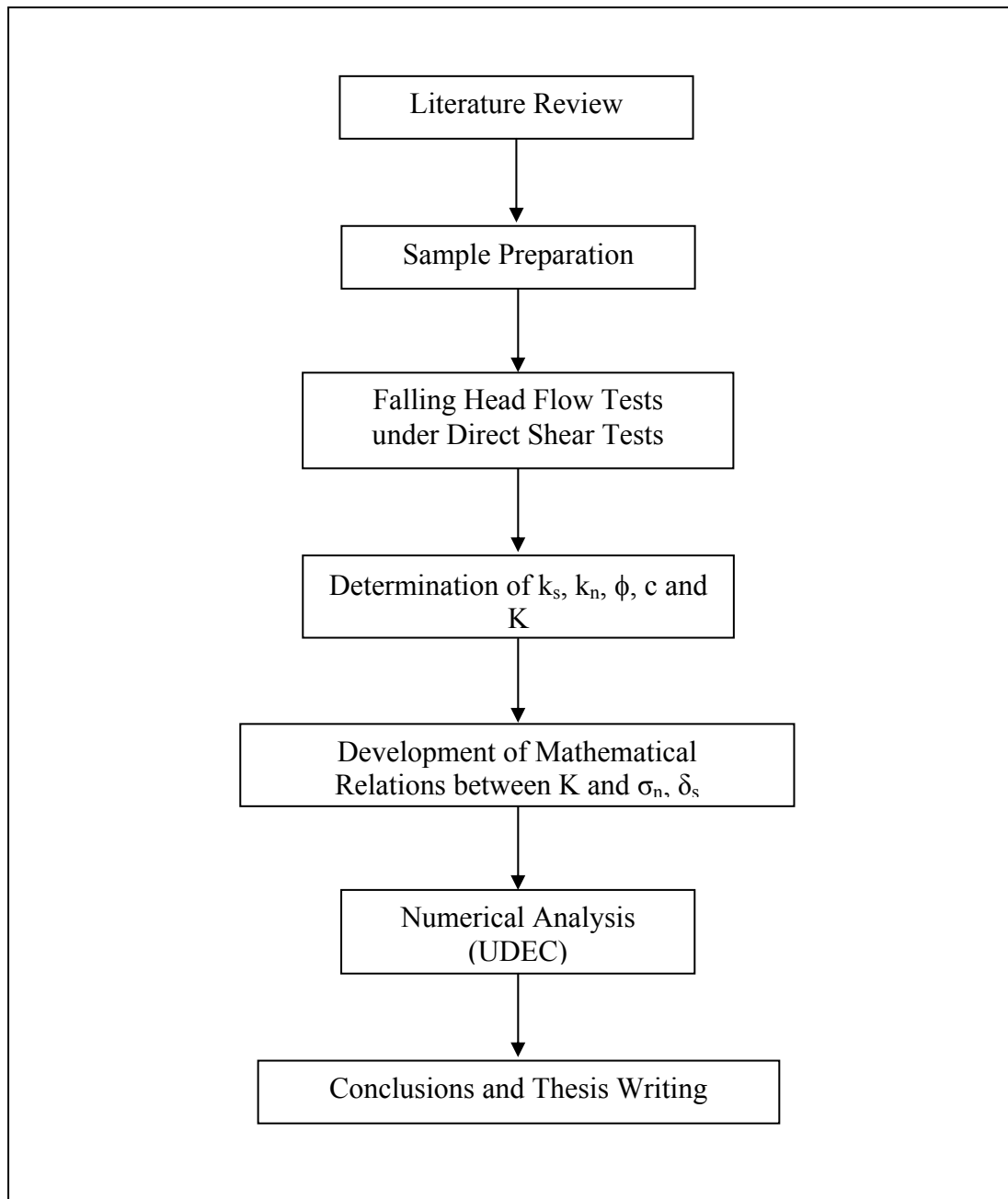
Figure 1.1 Research methodology

1.3.3 Falling head flow testing

Falling head tests are conducted by injecting water into the center hole of rectangular blocks of sample. A fracture is created across the block specimen either by saw-cutting or tension inducing methods. An 8 mm center hole is drilled into the upper block of the sample to allow water flow through the fracture. Then the pair of tested sample blocks is placed in the shear box of the direct shear testing machine. The shear force is applied while the flow testing is continued. The constant normal stresses on the fracture are varied from 1 to 4 MPa by using loading devices. The test is terminated when a total of 10 mm of shear displacement is reached. A minimum of 4 samples for each rock type are tested.

1.3.4 Determination of k_s, k_n, ϕ, c and K

Test results are used to determine the joint normal stiffness, the joint shear stiffness from stress and displacement relations and to calculate friction angle and cohesion form normal and shear stress relations.

1.3.5 Development of mathematical relations and flow equations

Results from laboratory measurements in terms of rock fracture permeability, fractures aperture, stress states and shear displacement are used to formulate mathematical relations.

1.3.6 Numerical analysis

The numerical modeling in this research aims at studying the deformation and failure behavior of fractured rock mass around excavations. Finite different analysis using UDEC code are performed to simulate the permeability increase zone near excavations.

1.3.7   Conclusions and thesis writing

All research activities, methods, and results are documented and complied in the thesis.

1.4   Scope and limitations of the study

The scope and limitations of the research include as follows.

1. Laboratory experiments will be conducted on specimens from four samples including Saraburi marble, Tak granite, Vietnamese granite and Chinese granite.

2. Testing on fractures will be made under normal stresses ranging from 1 to 4 MPa.

3. All tested fractures will be artificially made in the laboratory with a nominal area of $10{\times}10$ cm^2.

4. Fracture permeability is determined by falling head flow testing.

5. All tests will be conducted under ambient temperature.

6. Up to 4 samples will be tested for each rock type.

7. Water will be used as flow medium.

8. No field testing will be conducted.

9. X-ray diffraction analysis will be performed to determine the mineral compositions of the tested rocks.

1.5   Thesis contents

Chapter I introduces the thesis by briefly describing the background of problems and significance of the study. The research objectives, methodology, scope and limitations are identified. **Chapter II** summarizes results of the literature review.

Chapter III describes the sample preparation and laboratory experiment. **Chapter IV** presents the results obtained from the laboratory testing. **Chapter V** describes the numerical modeling to predict the hydraulic conductivity of rock around opening by UDEC. **Chapter VI** concludes the research results, and provides recommendations for future research studies. **Appendix A** provides detailed results of direct shear testing. **Appendix B** provides detailed of technical publication.

CHAPTER II

LITERATURE REVIEW

2.1 Introduction

This chapter summarizes the results of literature review carried out to improve an understanding of simulation of rock slope failure using physical model. The topics reviewed here include the fluid flow in fracture rock, permeability of fracture rock, and stiffness of fracture.

2.2 Literature review

Stress Effects on Fracture Void Geometry

Deformation in a fracture can arise from either a change in fluid pressure or a perturbation of the stress field in the rock. The important stress for mechanical behavior and fluid flow in fractures is the effective stress, which is generally taken to be the normal stress on the fracture minus the fluid pressure (Terzaghi, 1936).

The stress on a fracture can be decomposed into two components; one in a direction perpendicular to the surface (normal) and one in a direction parallel the surface (shear). In general, the effects of these two components are highly coupled; that is, the deformation caused by a change in one component is dependent on the magnitude of the other. Fracture surface roughness is one of the primary reasons for this coupling, as illustrated in Figure 1. This figure shows the distribution of voids and contacting asperities in an idealized representation of a very rough undeformed
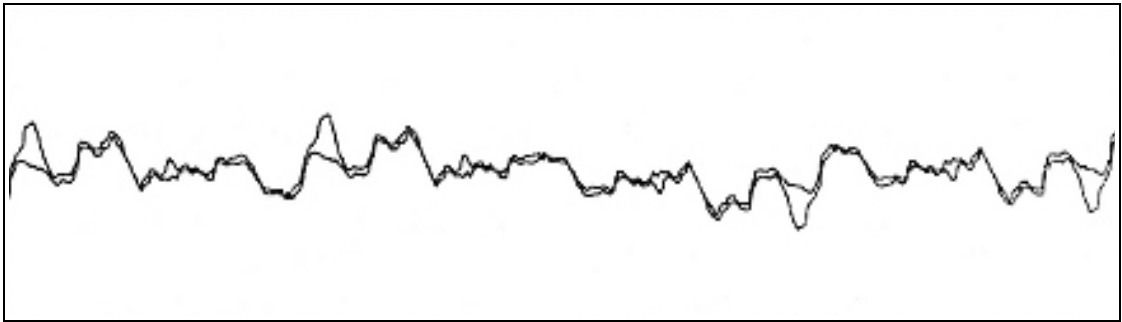
Figure 2.1 Cross section through a very rough fracture in the undeformed

state showing distribution of voids and contacting asperities

(National Research Council, 1996).

fracture. The application of shear stress to this fracture at a very low normal stress

may cause one surface to ride up and over the asperities of the other, leading to large

dilation. At the other extreme, at very high normal stress, the frictional forces resisting

slip may exceed the strength of the rock and the asperities will be sheared off. Dilation

would minimal in this case (National Research Council, 1996).

Baghbanan and Jing (2008) studied the effect of stress on permeability and

fluid flow patterns in fractured rock masses when distributed fracture aperture is

correlated with fracture trace length, using a discrete element method (DEM). The

basic assumptions are that the rock matrix is impermeable and linearly elastic, and that

the fluid flows only in fractures. The results show that when small stress ratios (K =

horizontal/vertical stress) are applied at the model boundaries, the overall permeability

of the fracture network is generally decreased. However, contribution from a few large

fractures of higher hydraulic conductivity prevents drastic reduction of the overall

permeability, compared with models that assume uniform fracture apertures. With

large values of the stress ratio, both the overall permeability and flow patterns are

controlled by a combination of highly conductive larger fractures and fractures with shear slipping and dilation, with much increased overall permeability and shear-induced flow channeling. These results show significant difference between correlated and non-correlated aperture and fracture length distributions, and highlight more significant scale and stress dependence of hydro-mechanical behavior of fractures rocks when geometric parameters of rock fractures are correlated.

Son et al. (2004) proposed a new constitutive model for the shear behavior of rough rock joints. Within the framework of the classical elasto-plastic theories, the model incorporates the dilation and surface degradation which are distinct features of rough rock joints. The elastic behavior is represented by the shear and normal stiffness. To calculate the plastic displacements after yielding, the non-associated flow rule is applied. Maksimovic's equation and Lee's empirical formula for joint shear strength are used for yield and plastic potential functions. The changes of the joint roughness angle that occurred in pre- and post-peak ranges of shear strength curve were approximated by simple power expressions of accumulated tangential plastic work. A joint finite element, which has 6-node and zero thickness, was used for implementing the proposed joint constitutive model. In order to evaluate the performance of the model, numerical direct shear tests were carried out. The results of the simulation confirmed that the proposed model could reproduce salient phenomena commonly observed in actual shear test of rock joints, including the shear strength hardening, softening, and dilation phenomena.

Baghbanan and Jing (2006) investigated permeability of fractured rocks considering the correlation between distributed fracture aperture and trace length, based on a newly developed correlation equation. The influence of the second moment

of the lognormal distribution of apertures on the existence of representative elementary volume (REV), and the possibility of equivalent permeability tensor of the fractured rock mass, is examined by simulating flow through a large number of stochastic discrete fracture network (DFN) models of varying sizes and varying fracture properties. The REV size of the DFN models increases with the increase of the second moment of the lognormal distribution, for both the correlated and uncorrelated cases. The variation of overall permeability between different stochastic realizations is an order of magnitude larger when the aperture and length are correlated than when they are uncorrelated. The mean square error of the directional permeability increases with increasing value of the second moment of the lognormal distribution function, and good fitting to an ellipsis of permeability tensor can only be reached with very large sizes of DFN models, compared with the case of constant fracture aperture, regardless of fracture trace length.

Pyrak-Noltea and Morrisa (2000) stated that fracture specific stiffness and fluid flow through a single fracture under normal stress are implicitly related through the geometry of the void space and contact area that comprise the fracture. Data from thirteen difference rock samples, each containing a single fracture, show that relationships between fracture specific stiffness and fluid flow through a fracture fall into two general classes of behavior. Fractures either fall on a loosely-defined universal curve relating fluid flow to fracture specific stiffness, or else the flow is weakly dependent on fracture specific stiffness. The second relationship shows that flow decreases slowly with increasing fracture specific stiffness. The first relationship shows that flow decreases rapidly for increases in fracture specific stiffness. To understand this behavior, computer simulations on simulated single fractures were

performed to calculate fluid flow, fracture displacement, and fracture specific stiffness as a function of normal stress. Simulated fractures with spatially correlated and uncorrelated aperture distributions were studied. Fractures with spatially uncorrelated aperture distributions tend to exhibit a weak dependence of fluid flow on fracture specific stiffness because these fractures tend to have multiple connected paths across the sample which can support flow with uniformly distributed contact area. Thus an increment in stress will increase the stiffness of the fracture without greatly reducing the amount of fluid flow. On the other hand, fractures with spatially correlated aperture distributions tend to belong to the universal relationship because correlated fractures tend to have only one or two dominant flow paths and the contact area is limited to a few regions resulting in a compliant fracture. Thus an increment in stress on a spatially correlated fracture will result in an increase in stiffness and rapid decrease in fluid flow. These spatial correlations in fracture void geometry can be differentiated in the laboratory based on the observed fracture specific stiffness-fluid flow relationship for a single fracture under normal loading.

Auradou et al. (2006) investigated the effect on the transport properties of a fracture of a shear displacement u between its complementary surfaces experimentally and numerically. The shear displacement u induces an anisotropy of the fracture aperture field with a correlation length scaling of $|u|$, which is significantly larger in the direction perpendicular to u. This reflects the presence of long fluid flow channels perpendicular to the shear displacement, resulting in a higher effective permeability in that direction. Such channels will have a strong influence on the transport characteristics of a fracture, such as, for instance, its thermal exchange area, crucial for geothermal applications. Miscible displacement fronts in shear-displaced

fractures obtained experimentally display a self-affine geometry with a characteristic exponent directly related to that of the fracture surfaces. They present a simple model, based on the channeling of the aperture field, which reproduces the front geometry when the mean flow is parallel to the channels created by the shear displacement.

Giacominia et al. (2008) investigated the flow anisotropy within a natural joint subjected to mechanical shear. The cubic law is the simplest way to describe fluid flow through rock joints but because of rock wall roughness, deviations from this model have been observed. The Reynolds equation usually gives better results. In this study, micro-scale roughness is taken into account to define a reduced coefficient of permeability. Numerical simulations have been carried out by applying Darcy's law to the rock joint, described as an equivalent porous medium. The numerical simulations are based on experimental data obtained by Hans (2002) from a series of hydromechanical shear tests on a rock joint replica. The numerical results have been compared to the experimental ones, and to the results obtained by applying the Reynolds equation, to assess the relevance of the simulations. For the fracture studied, the approach proposed herein can reproduce relatively well the experimental flow anisotropy, and provides consistent values of flow rates, whereas the Reynolds equation tends to give higher flow rates.

Hamiel et al. (2005) stated that the dilation of rock under shear gives rise to detectable effects both in laboratory experiments and in field observations. Such effects include hardening due to reduction in pore pressure and asymmetrical distribution of deformation following strike slip earthquakes. They examine the nonlinear poroelastic behavior of isotropic rocks by a new model that integrates Biot's classic poroelastic formulation together with nonlinear elasticity, and apply it to

Coulomb failure criterion and pore pressure response to a fault slip. They investigate the poroelastic response of two alternative forms of a non-Hookean secondorder term incorporated in the poroelastic energy. This term couples the volumetric deformation with shear strain. Like linear poroelasticity, our model shows an increase of pore pressure with mean stress (according to Skempton coefficient B) under undrained conditions. In addition, in their model pore pressure varies also with deviatoric stresses, where rising deviatoric stresses (at constant mean stress) decreases pore pressure (according to Skempton coefficient A), due to dilatancy. The first version of our model is consistent with a constant A smaller than 1/3, which is in agreement with the classic work of Skempton, but does not fit well the measured undrained response of sandstones. The second model allows A and B to vary with shear stress, and displays the experimentally observed connection between pore pressure and deviatoric stresses under undrained conditions in Berea and Navajo sandstone samples. Numerical results predict dilatancy hardening and suggest that it should be taken into consideration in Coulomb failure stress calculations. They apply our model to the distribution of pore pressure changes in response to a fault slip. Results of numerical simulations of coseismic deformation demonstrate that due to dilatancy regions of decreasing pore pressure are larger relative to regions of increasing pore pressure. The model predictions have significant implications for coseismic water level changes and post-seismic pore pressure diffusion and crustal deformation.

Jiang et al. (2004) study evaluations of shear strength and flow behavior of rock joints play an important role in designing of deep underground openings and in performing underground waster disposal risk assessments. Although shear strength and flow behavior can be investigated in a laboratory using a direct shear apparatus,

the experimental results are influenced by boundary conditions and the simulation conditions may not be representative of the field conditions. This paper introduces a newly developed automated servo-control hydro-mechanical direct shear apparatus that is capable of automatically adjusting the normal stiffness according to the deformational capacity of the surrounding rock masses, thereby accurately simulating the high pressure head in deep underground locations. The proposed apparatus was used to perform shear tests on artificial joint specimens. Experimental measurements of the coupled mechanical and hydraulic behavior of rock joints under CNL and CNS conditions were analyzed. The shear strength and permeability results exhibited a regular variation due to the interaction of the joint roughness and gouge production. The rock joint permeability results can be applied to deep underground construction.

Lee and Cho (2002) built a hydro-mechanical testing system, which is capable of measuring both the flow rates and the normal and shear displacement of a rock fracture, was built to investigate the hydraulic behavior of rough tension fractures. Laboratory hydraulic tests in linear flow were conducted on rough rock fractures, artificially created using a splitter under various normal and shear loading. Prior to the tests, aperture distributions were determined by measuring the topography of upper and lower fracture surfaces using a laser profilometer. Experimental variograms of the initial aperture distributions were classified into four groups of geostatistical model, though the overall experimental variograms could be well fitted to the exponential model. The permeability of the rough rock fractures decayed exponentially with respect to the normal stress increase up to 5 MPa. Hydraulic behaviors during monotonic shear loading were significantly affected by the dilation occurring until the shear stress reached the peak strength. With the further dilation, the permeability of

the rough fracture specimens increased more. However, beyond shear displacement of about 7 to 8 mm, permeability gradually reached a maximum threshold value. The combined effects of both asperity degradation and gouge production, which prohibited the subsequent enlargement of mean fracture aperture, mainly caused this phenomenon. Permeability changes during cyclic shear loading showed somewhat irregular variations, especially after the first shear loading cycle, due to the complex interaction from asperity degradations and production of gouge materials. The relation between hydraulic and mechanical apertures was analyzed to investigate the valid range of mechanical apertures to be applied to the cubic law.

Akkrachattrarat et al. (2009) discussed the hydraulic conductivity of fractures in sandstone specimens under normal and shear stresses. The effort primarily involves performing series of falling head flow tests on tension-induced fractures in four types of sandstone samples. The tested sandstones belong to the Phu Phan, Sao Khua, Phu Kradung and Pra Wihan formations of the Khorat group. The changes of the physical and hydraulic apertures, the water flow rates, and the applied shear stresses are monitored and used to calculate the changes of the fracture permeability as a function of shear displacement. The results indicate that the physical aperture e_p and hydraulic aperture e_h increase with shearing displacement, particularly under high normal stresses. The magnitudes of fracture permeability under no shear and under peak shear stress are similar. For both peak and residual regions, the physical apertures are about 5 to 10 times greater than the hydraulic apertures, as a result the fracture hydraulic conductivity determined from the physical aperture are about one to two orders of magnitudes greater than these determined from the equivalent hydraulic apertures. This is probably because the measured physical apertures do not consider the effect of

fracture roughness that causes a longer flow path. The difference between the permeability under residual shear stress and that under peak stress becomes larger under higher normal stresses. The fracture hydraulic conductivities exponentially decrease with increasing the normal stresses. Their permeability is in the range between 0.1×10^{-3} m/s and 10×10^{-3} m/s.

Kemthong, R., and Fuenkajorn, K. (2007) performed direct shear testing on saw-cut specimens to determine the relationship between the basic friction angle (ϕ_b) and the rock compressive strength (UCS). Testing on specimens with tension-induced fractures yielded joint shear strengths under different JRC's for use in the verification. The results indicate that Barton's criterion using the field-identified parameters can satisfactorily predict the shear strengths of rough joints in marble and sandstones, and slightly over-predicts the shear strength in the basalt specimens. It cannot however describe the joint shear strengths for the granite specimens. This is probably because the saw-cut surfaces for coarse-grained and strong crystalline rocks are very smooth resulting in an unrealistically low ϕ_b. Barton's shear strength criterion is more sensitive to ϕ_b than to UCS and JRC. For all sandstones the ϕ_b values are averaged as 33 ± 8 degrees, apparently depending on their cementing materials. The average ϕ_b for the tested marbles and for the limestone recorded elsewhere 35 ± 3 degrees, and is independent of UCS. The ϕ_b values for other rock types apparently increase with UCS particularly for very strong rocks. The factors governing ϕ_b for crystalline rocks are probably crystal size, mineral compositions, and the cutting process, and for clastic rocks are grain size and shape and the strength of cementing materials.

Suanprom et al. (2009) performed flow tests to determine hydraulic conductivity of tension-induced fractures in sandstones under normal and shear stresses. The results indicate that the physical aperture e_p and hydraulic aperture e_h increase with shearing displacement, particularly under high normal stresses. The magnitudes of fracture permeability under no shear and under peak shear stress are similar. For both peak and residual regions, the physical apertures are about 5 to 10 times greater than the hydraulic apertures, as a result the fracture hydraulic conductivity determined from the physical aperture are about one to two orders of magnitudes greater than these determined from the equivalent hydraulic apertures. This is probably because the measured physical apertures do not consider the effect of fracture roughness that causes a longer flow path. The difference between the permeability under residual shear stress and that under peak stress becomes larger under higher normal stresses. The fracture hydraulic conductivities exponentially decrease with increasing the normal stresses. Their permeability is in the range between 0.1×10^{-3} m/s and 10.0×10^{-3} m/s.

CHAPTER III

# SAMPLE PREPARATION

This chapter describes the rock sample preparation. The rock samples include Saraburi marble, Tak granite, Vietnamese granite and Chinese granite (hereafter designated as SMB, TGR, VGR, CGR) (Figure 3.1). These rocks have significant impacts on stability of many engineering structures constructed in the region (e.g., slope embankments, underground mines and tunnels). They are selected here due to their uniform texture and availability.

A minimum of 4 samples are prepared for each rock type. The sample preparation is carried out in the laboratory at the Suranaree University of Technology. Samples for the falling head test are prepared to have fractures area of about 10×10 square centimeters. The fractures are artificially made by applying a line load to induce a splitting tensile crack in $10 \times 10 \times 7.6$ cm prismatic blocks of rocks samples (Figure 3.2). Their roughness is observed and classified by comparing with a reference profiles given by Barton (joint roughness coefficient – JRC, Barton, 1973). Table 3.1 shows the results of the joint roughness classification. Table 3.2 summarizes the results, including rock names, brief mineral compositions (Kemthong, R., and Fuenkajorn, K., 2007).
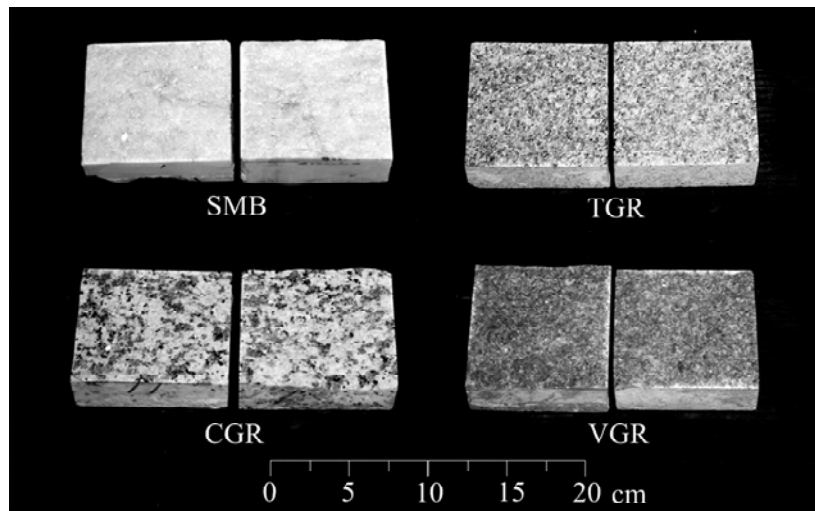
Figure 3.1 Some rock specimens prepared for falling head test under normal

and shear stresses.
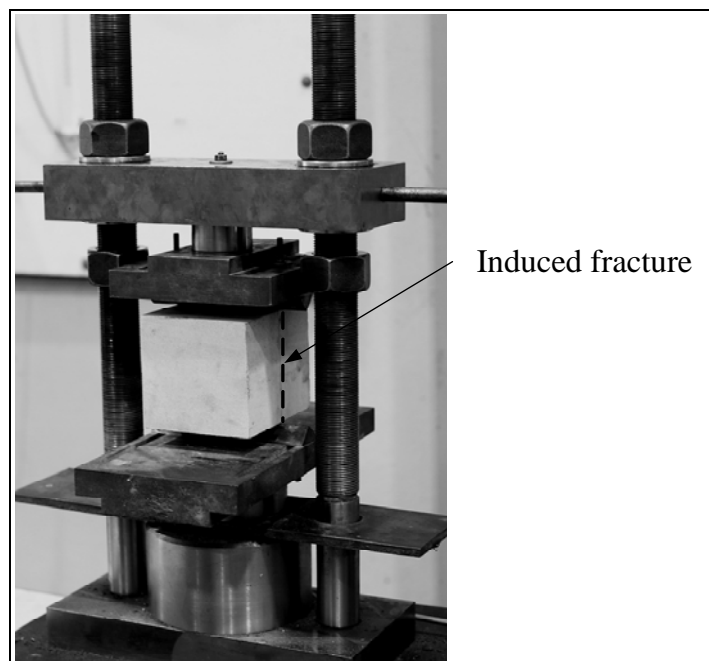
Induced fracture

Figure 3.2 A 10×10×7.6 cm block of rock sample is line-loaded to induce

tensile fracture in mid-length of the block

Table 3.1 The results of the joint roughness classification.

Sample No.	JRC	Sample No.	JRC
SMB-DS-01	9	CGR-DS-01	11
SMB-DS-03	11	CGR-DS-03	11
SMB-DS-04	11	CGR-DS-04	13
SMB-DS-06	9	CGR-DS-05	15
TGR-DS-01	11	VGR-DS-01	15
TGR-DS-02	11	VGR-DS-03	13
TGR-DS-04	11	VGR-DS-04	15
TGR-DS-05	11	VGR-DS-06	17

Table 3.2 Mineral compositions of tested rock samples (Kemthong, R., and

Fuenkajorn, K., 2007).

| Rock Name	Code	Mineral compositions
Saraburi Marble	SMB	100% Calcite (1-5 mm)
Tak Granite	TGR	40% Plagioclase (0.5-1 mm), 30% quartz (2-5 mm), 5% orthoclase (3-5 mm), 3% amphibole (1-2 mm), and 2% biotite
Vietnamese Granite	VGR	75% Orthoclase (0.3-2 cm), 10% quartz (2-5 mm), 10% plagioclase (1-3 mm), and 5% amphibole (1-2 mm)
Chinese Granite	CGR	70% Plagioclase (0.5-2 cm), 15% quartz (3-5 mm), 7% orthoclase (2-3 mm), 5% amphibole (1-2 mm), and 3% biotite (2-3 mm)

CHAPTER IV

# LABORATORY TESTING

4.1   Introduction

The objective of the laboratory testing is to determine the permeability of rock fractures under shearing stresses and displacements. This chapter describes the method and results. The changes of the physical and hydraulic apertures, the water flow rates, and the applied shear stresses are monitored and used to calculate the changes of the fracture permeability as a function of shear displacement.

4.2   Test method

Falling head tests are conducted by injecting water into the center hole of rectangular blocks of sample. Figures 4.1 and 4.2 show the laboratory arrangement of the falling head flow test while the fracture is under normal and shear stresses. The maximum water head above the tested fracture is 1.23 m. The injection hole at the center of the lower block is 0.8 cm in diameter. The fractures are artificially made by applying a line load to induce a splitting tensile crack in 10×10×7.6 cm prismatic blocks of rocks samples. The fracture area is 10×10 cm. Their roughness is observed and classified by comparing with a reference profiles given by Barton (joint roughness coefficient – JRC, Barton, 1973). The constant normal stresses are 0.35, 1.03, 2.07 and 3.10. MPa. The shear stress is applied while the shear displacement and head drop are monitored for every 0.5 mm shear displacement. The maximum shear displacement
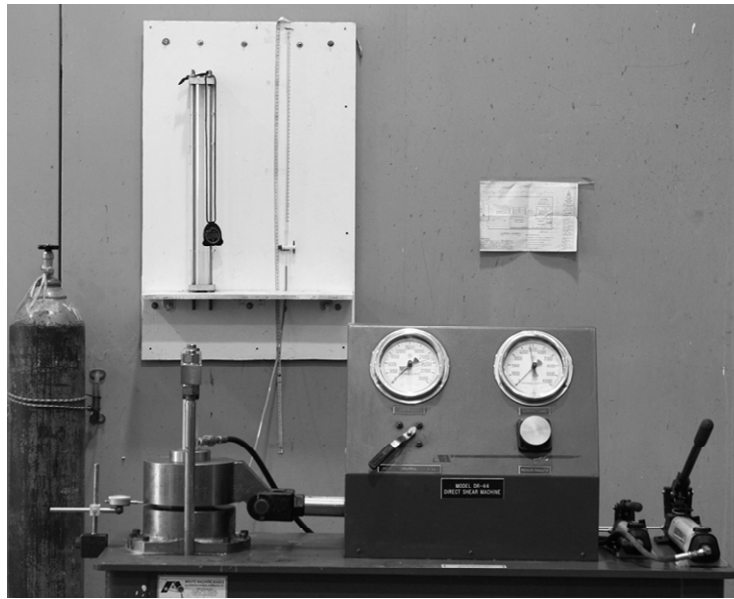
Figure 4.1 Laboratory arrangements for falling head flow tests
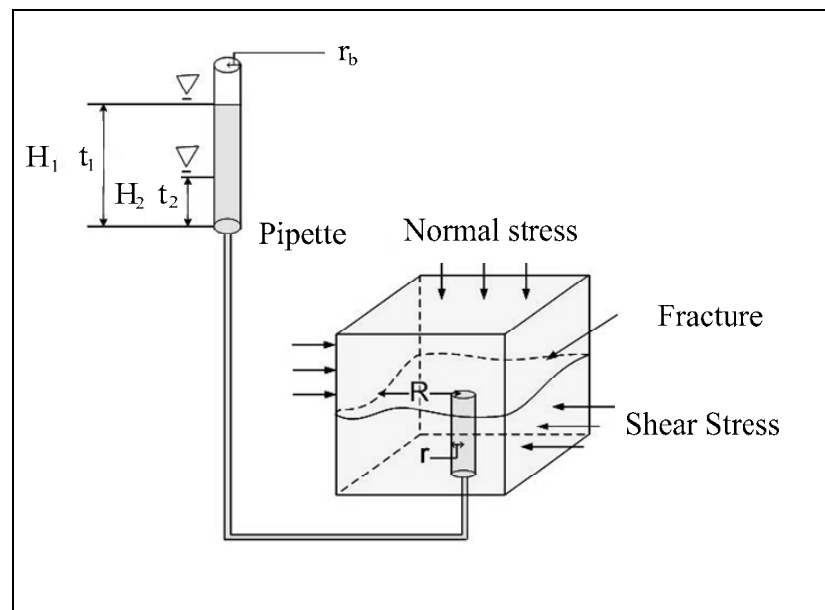
Figure 4.2 Laboratory arrangements for falling head test under normal

and shear stresses.

is 10 mm. The (physical) fracture aperture is measured to the nearest 0.01 mm before and after normal and shear stress application. The fracture dilations are also monitored during the shear test.

The physical, mechanical and hydraulic apertures are used to calculate the hydraulic conductivity of the tested fractures. The physical aperture (e_p) is obtained from the actual measurements of the fractures before and during normal and shear stress applications. The measurement points are at the four corners of the shear box. The physical aperture at each shear displacement is an average from the four measurements. The mechanical aperture (e_m) in mm is calculated by (Barton and Bakhtar, 1983; Bandis et al., 1983, 1985):

$$e_m = [JRC/5] / [0.2(\sigma_c/JCS) - 0.1] \qquad (4.1)$$

where σ_c is the uniaxial compressive strength of the rock (MPa), JCS is joint compressive strength of the rock (MPa). Here σ_c and JCS are assumed to be equal. The measured JRC values range from 9, 11, 13 and 15. From equation (4.1) the equivalent mechanical apertures for the above JRC values are 180, 220, 260 and 300 micro-meters.

The equivalent hydraulic aperture (e_h) for radial flow is calculated by (Maini, 1971):

$$e_h = [[\ln(H_1 / H_2)r_b^2 \ln(R / r)6\mu] / [(t_2 - t_1)\gamma]]^{1/3} \qquad (4.2)$$

where γ is unit weight of water (N/m^2), μ is dynamic viscosity (N·s/m^2), H_1, H_2 is water heads at t_1 and t_2, r_b is pipette radius (m), R is radius of flow path (m), r is radius of the radius injection hole (m).

The fracture permeability is calculated by (Zeigler, 1976):

$$K = \gamma e^2 / 12\mu \tag{4.3}$$

where K is hydraulic conductivity between smooth and parallel plates, e is parallel plate aperture. It is assumed here that the flow is isotropic across the fracture plane, and that the intact rock is impermeable.

Here the fracture conductivity is calculated for three types of fracture apertures: e_p, e_m and e_h, and differentiated by different symbols as K_p – physical, K_m – mechanical, and K_h – hydraulic conductivities.

The joint shear stiffness for various normal stresses is calculated at the 50% peak stress using an equation (Indraratna and Ranjith, 2001):

$$k_s = \tau_s/\delta_s \tag{4.4}$$

where K_s is the joint shear stiffness (MPa/m), τ_s is the shear stress (MPa), δ_s is the shear displacement (m).

The normal stiffness of fractured is calculated by (Indraratna and Ranjith, 2001):

$$k_n = \sigma_n/\delta_n \tag{4.5}$$

where K_n is the joint normal stiffness (MPa/m), τ_n is the normal stress (MPa), δ_n is the normal displacement (m).

Table 4.1 summarizes the results of the fracture stiffness calculations for Saraburi marble, Tak granite, Vietnamese granite and Chinese granite. The fracture stiffness determined here compare well with these obtained by (Pyrak-Nolte et al., 2000). The joint shear stiffness tends to increase with the normal stresses.

Table 4.1 Normal and shear stiffness of rock samples.

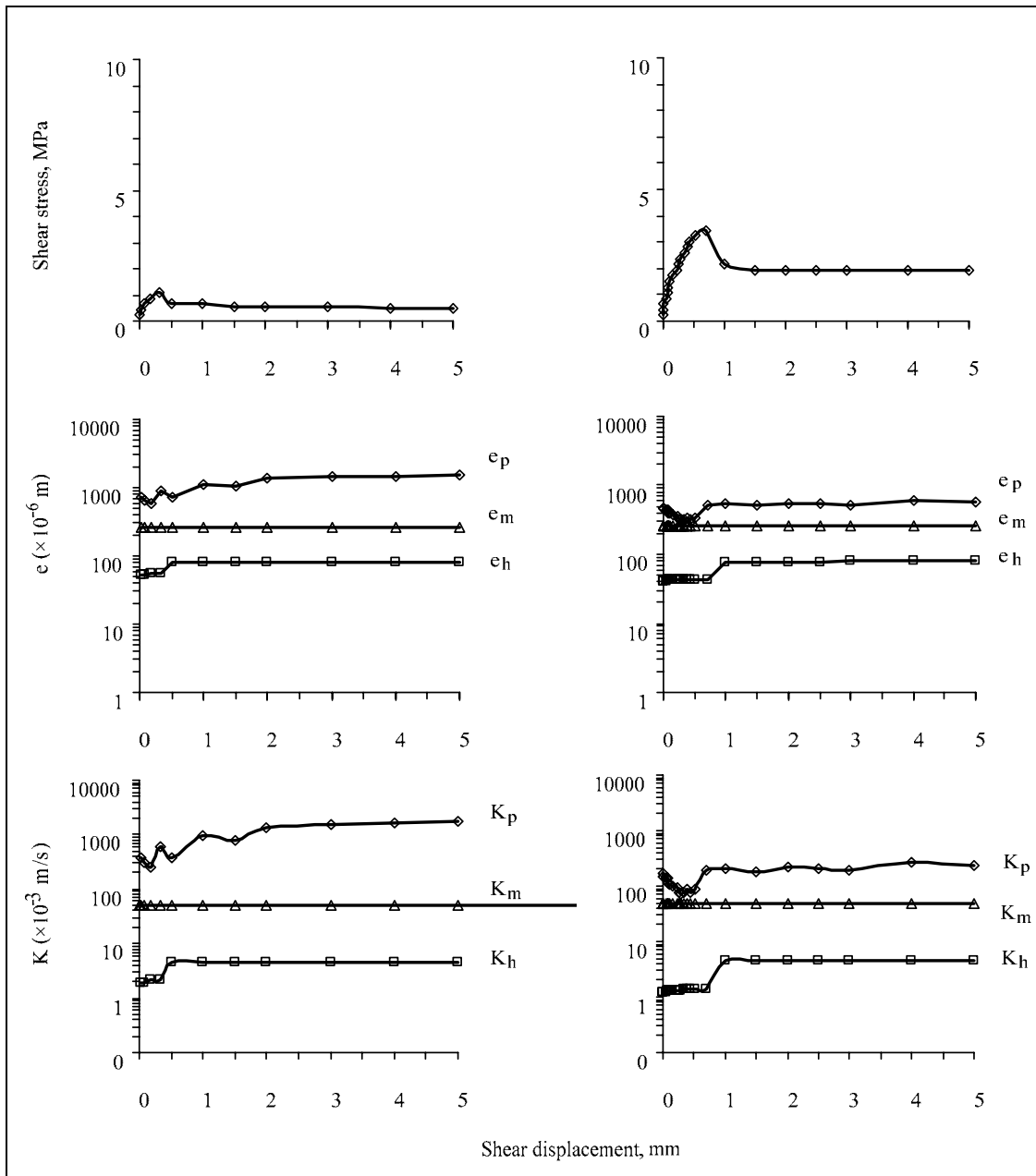| Specimen No.	σ_n(MPa)	K_s (GPa/m)	K_n (GPa/m)
SMB-DS-06	0.35	2.87	5.6
SMB-DS-04	1.03	5.77	2.68
SMB-DS-03	2.07	14.92	2.72
SMB-DS-01	3.1	14.92	7.09
Average		9.62 ± 6.23	4.52 ± 2.19
TGR-DS-05	0.35	4.06	4
TGR-DS-04	1.03	12.58	2.35
TGR-DS-02	2.07	11.54	7.53
TGR-DS-01	3.1	17.92	4
Average		11.53 ± 5.71	4.47 ± 2.18
CGR-DS-03	0.35	7.19	0.39
CGR-DS-05	1.03	14.39	2.75
CGR-DS-01	2.07	14.68	3.57
CGR-DS-04	3.1	18.81	2.76
Average		13.77 ± 4.83	2.37 ± 1.37
VGR-DS-03	0.35	4.4	0.69
VGR-DS-06	1.03	7	3.32
VGR-DS-01	2.07	7.33	2.76
VGR-DS-04	3.1	8.6	6.08
Average		6.83 ± 1.76	3.21 ± 2.22

4.3   Test results

The fracture hydraulic conductivities are calculated for the three aperture measurements and plotted as a function of shear displacement (δ_s) for normal stresses (σ_n) of 0.35, 1.03, 2.07 and 3.10 MPa in Figures 4.3 through 4.10 for Saraburi marble (SMB), Tak granite (TGR), Vietnamese granite (VGR) and Chinese granite (CGR). They are also compared with their corresponding shear stress-shear displacement diagram (τ-δ_s). Since the shear stresses after the peak value remain relatively consistent through 10 mm displacement, up to 3 mm shear displacement is plotted in the figure.

The fracture permeability is calculated from the equivalent hydraulic aperture (e_h) and from the physical aperture (e_p) for the peak ($K_{h, peak}$, $K_{p, peak}$) and residual ($K_{h, residual}$, $K_{p, residual}$) stresses. The mechanical aperture, e_m before, during and after shearing therefore remains constant for each fracture. As a result the hydraulic conductivity K_m calculated from e_m is independent of the shearing displacement.

The physical aperture e_p tends to increase with shearing displacement. Its value fluctuates before the peak and tends to be more consistent in the residual stress region. The K_p values calculated from e_p subsequently show similar characteristics of the curves in the permeability-shear displacement diagram.

The hydraulic aperture e_h indirectly determined from the inflow rates also tends to increase with the shear displacement, particularly under high normal stresses. Even though K_p and K_h show similar characteristics of the curves in the permeability-shear displacement diagram, K_p is always about an order of magnitude greater than K_h, particularly in the residual shear region.

Figure 4.3 Shear stress, fracture aperture, and hydraulic conductivity as a function

of shear displacement (δ_s) at normal stress = 0.35 MPa (left) and

1.03 MPa (right) for Saraburi marble.
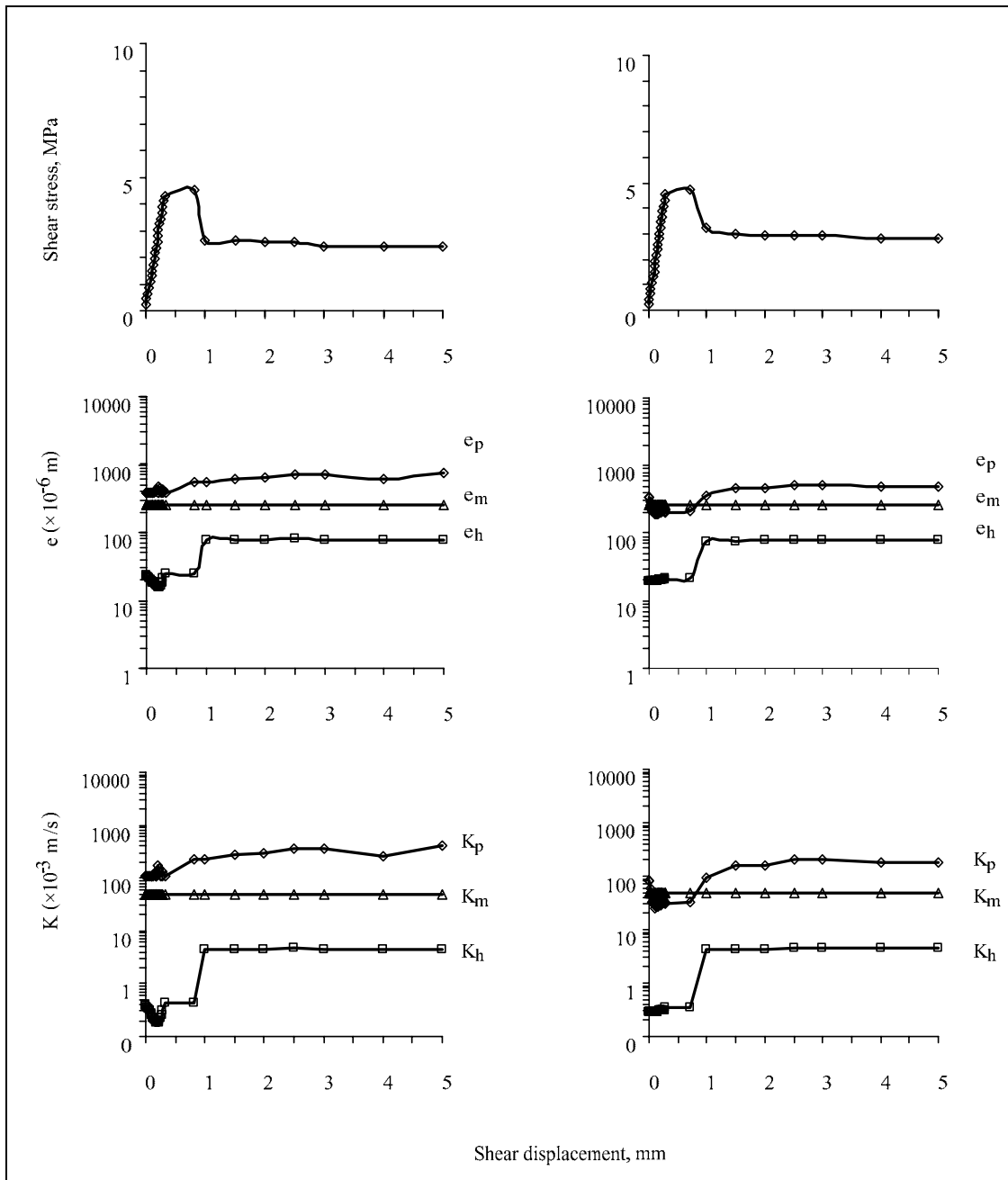
Figure 4.4 Shear stress, fracture aperture, and hydraulic conductivity as a function

of shear displacement (δ_s) at normal stress = 2.07 MPa (left) and
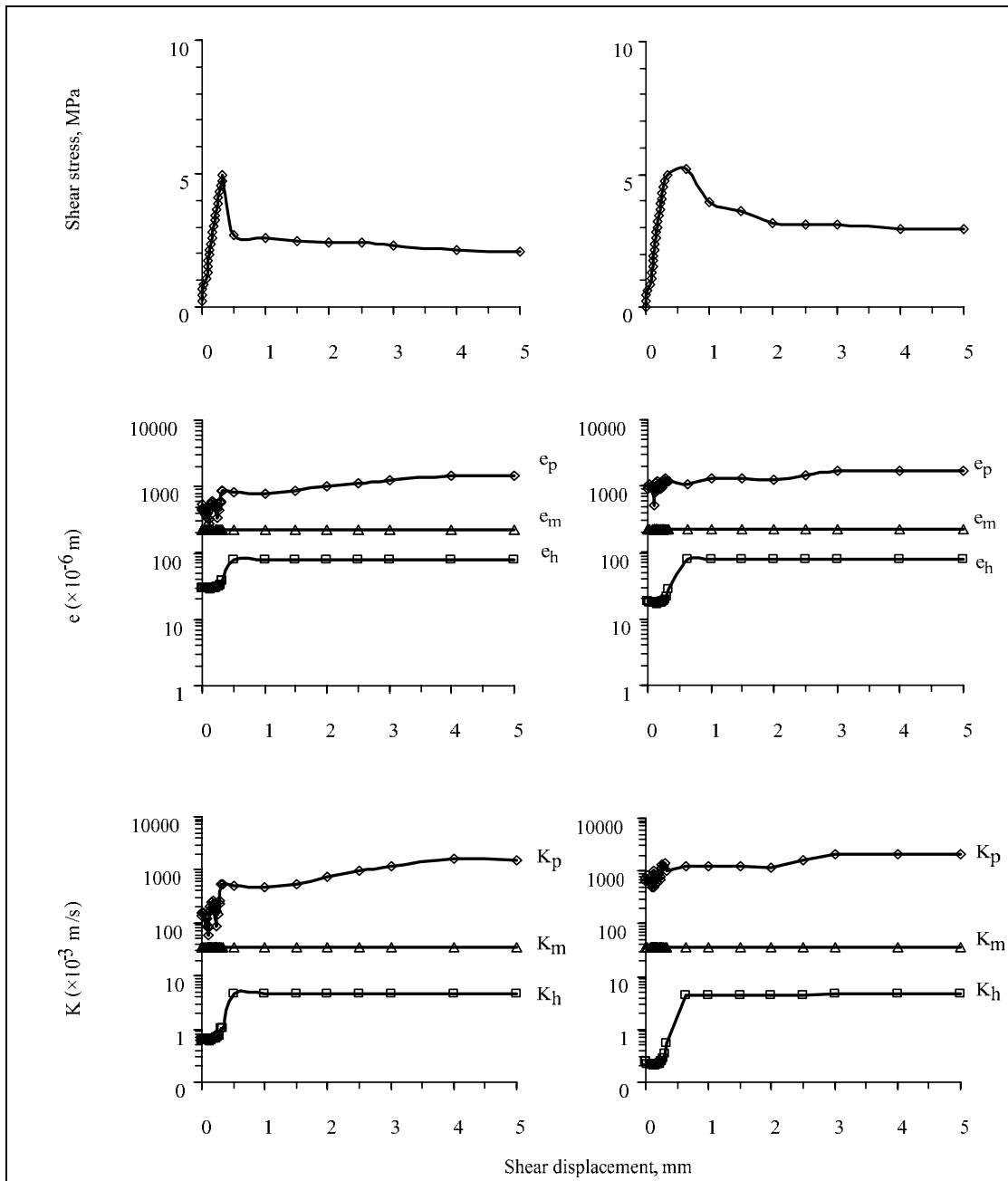
3.10 MPa (right) for Saraburi marble.
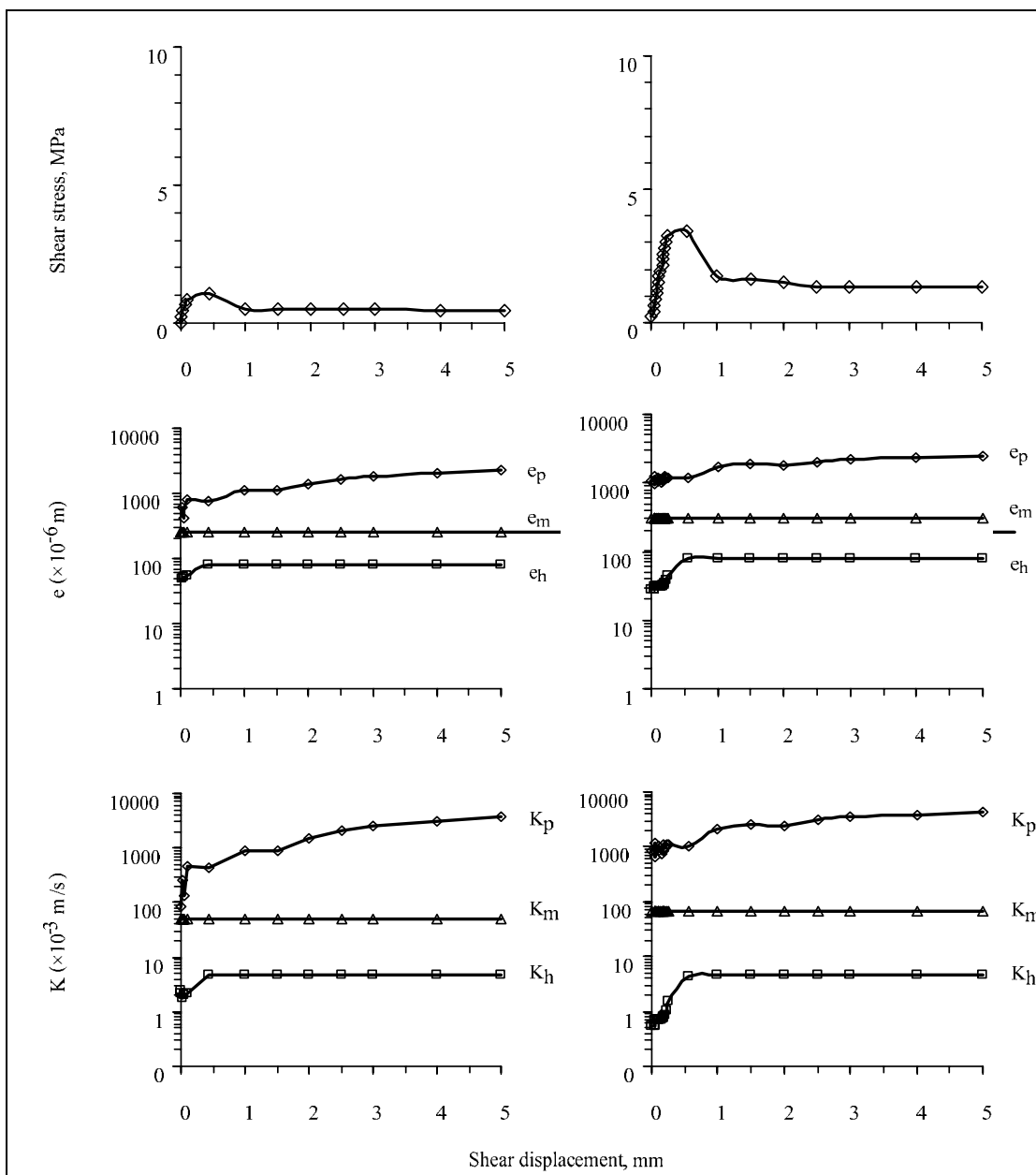
Figure 4.5 Shear stress, fracture aperture, and hydraulic conductivity as a function

of shear displacement (δ_s) at normal stress = 0.35 MPa (left) and

1.03 MPa (right) for Chinese granite.

Figure 4.6 Shear stress, fracture aperture, and hydraulic conductivity as a function

of shear displacement (δ_s) at normal stress = 2.07 MPa (left)

and 3.10 MPa (right) for Chinese granite.

Figure 4.7 Shear stress, fracture aperture, and hydraulic conductivity as a function

of shear displacement (δ_s) at normal stress = 0.35 MPa (left)

and 1.03 MPa (right) for Tak granite.

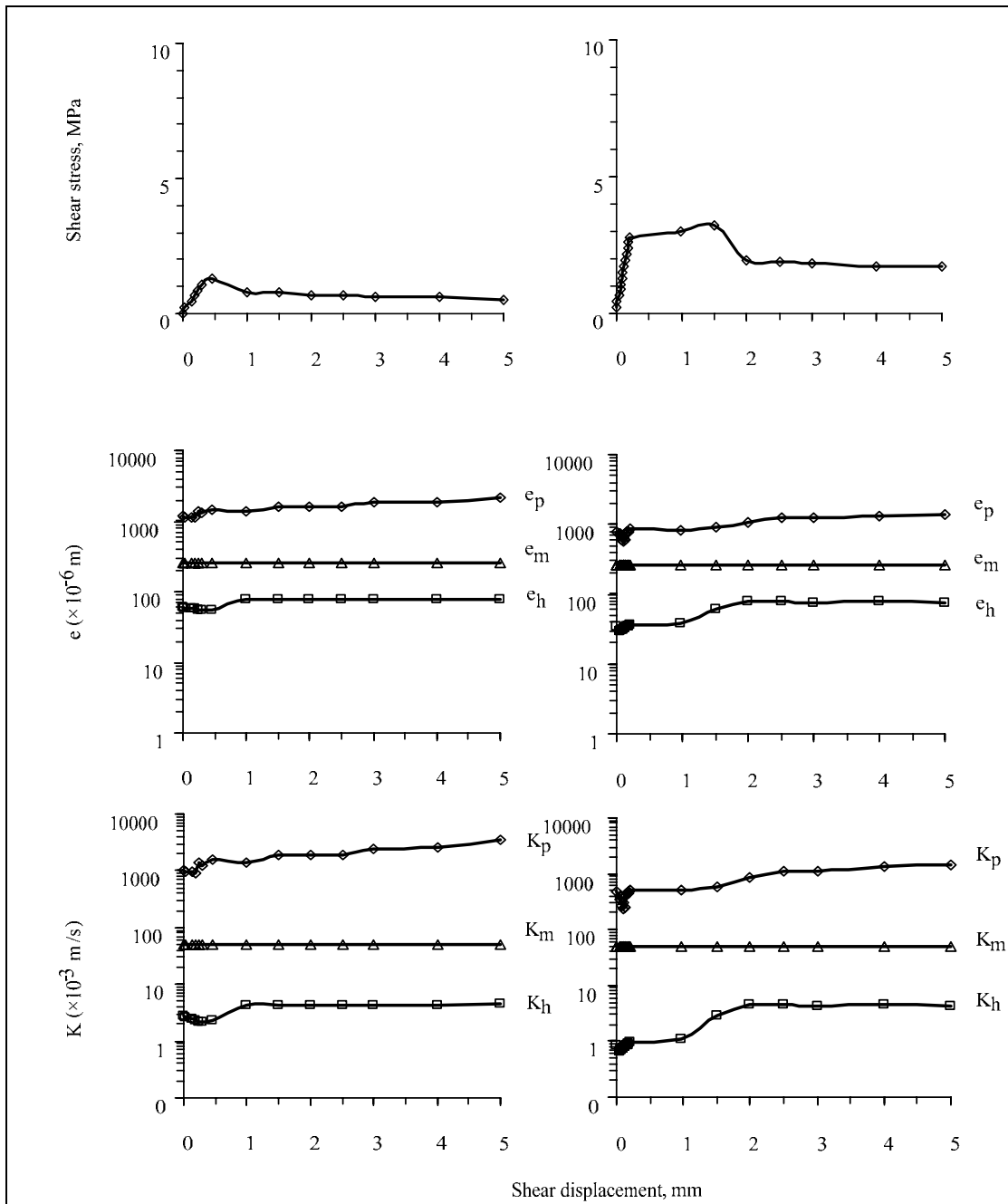**Figure 4.8** Shear stress, fracture aperture, and hydraulic conductivity as a function

of shear displacement (δ_s) at normal stress = 2.07 MPa (left)
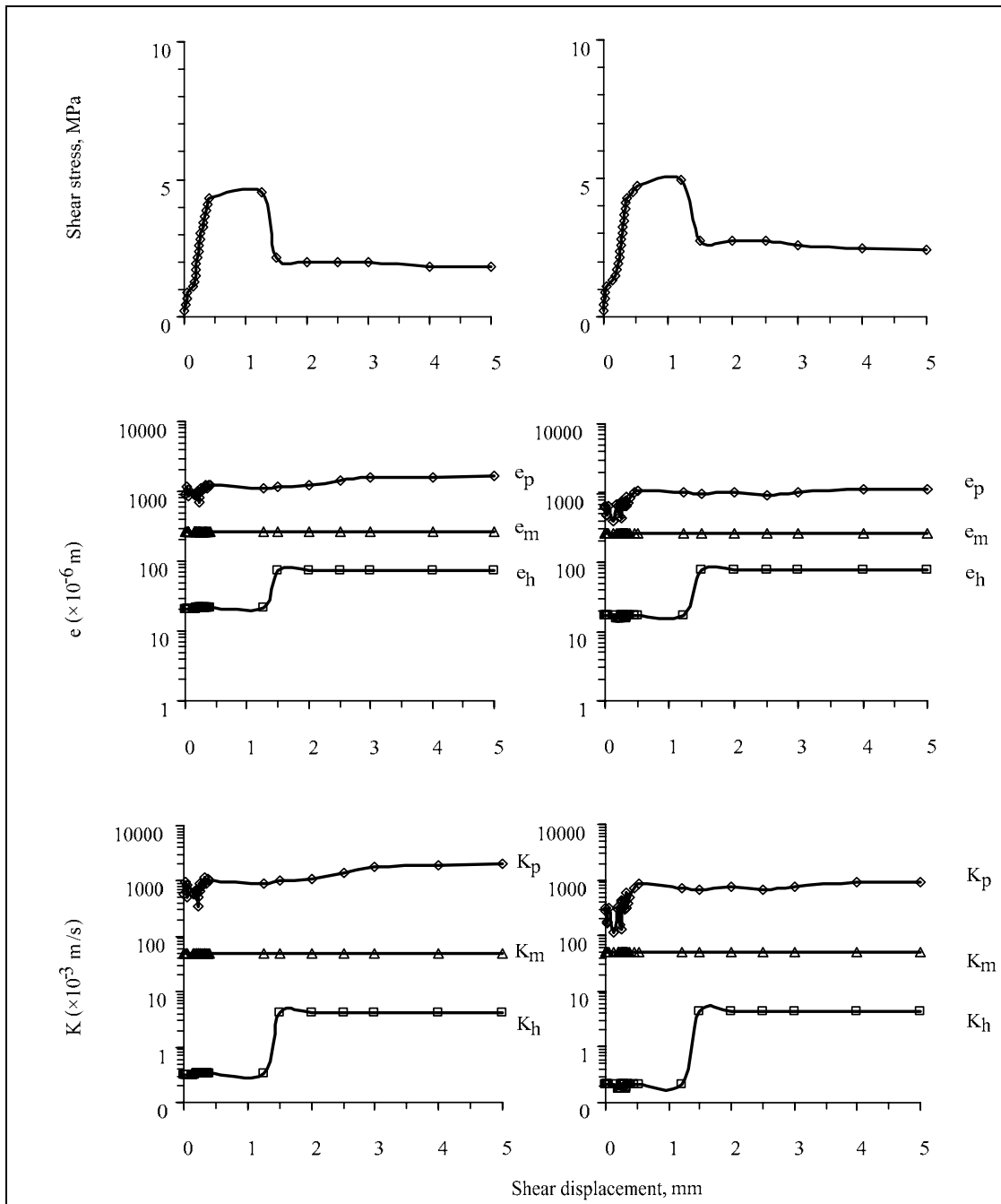
and 3.10 MPa (right) for Tak granite.

Figure 4.9 Shear stress, fracture aperture, and hydraulic conductivity as a function

of shear displacement (δ_s) at normal stress = 0.35 MPa (left)
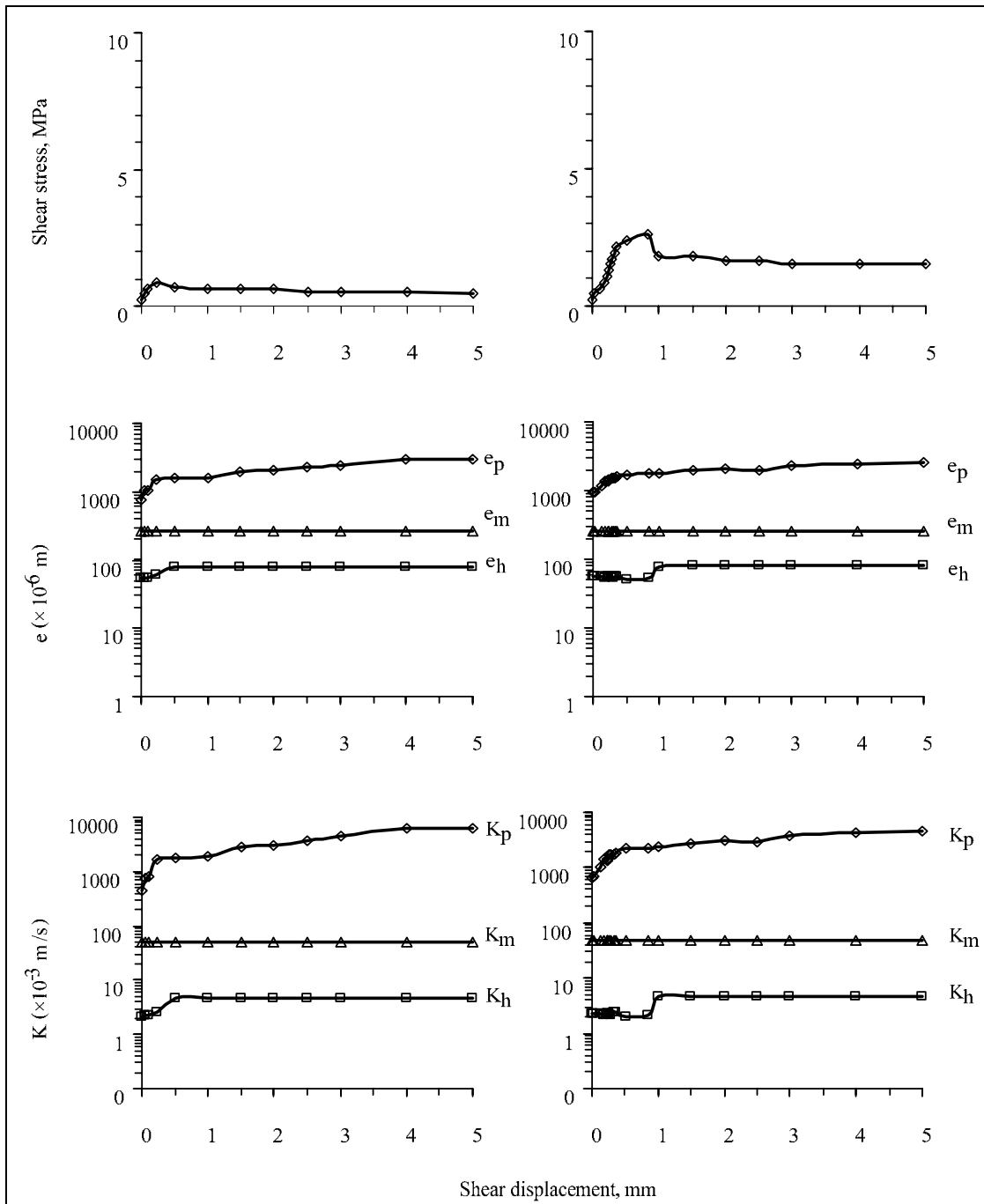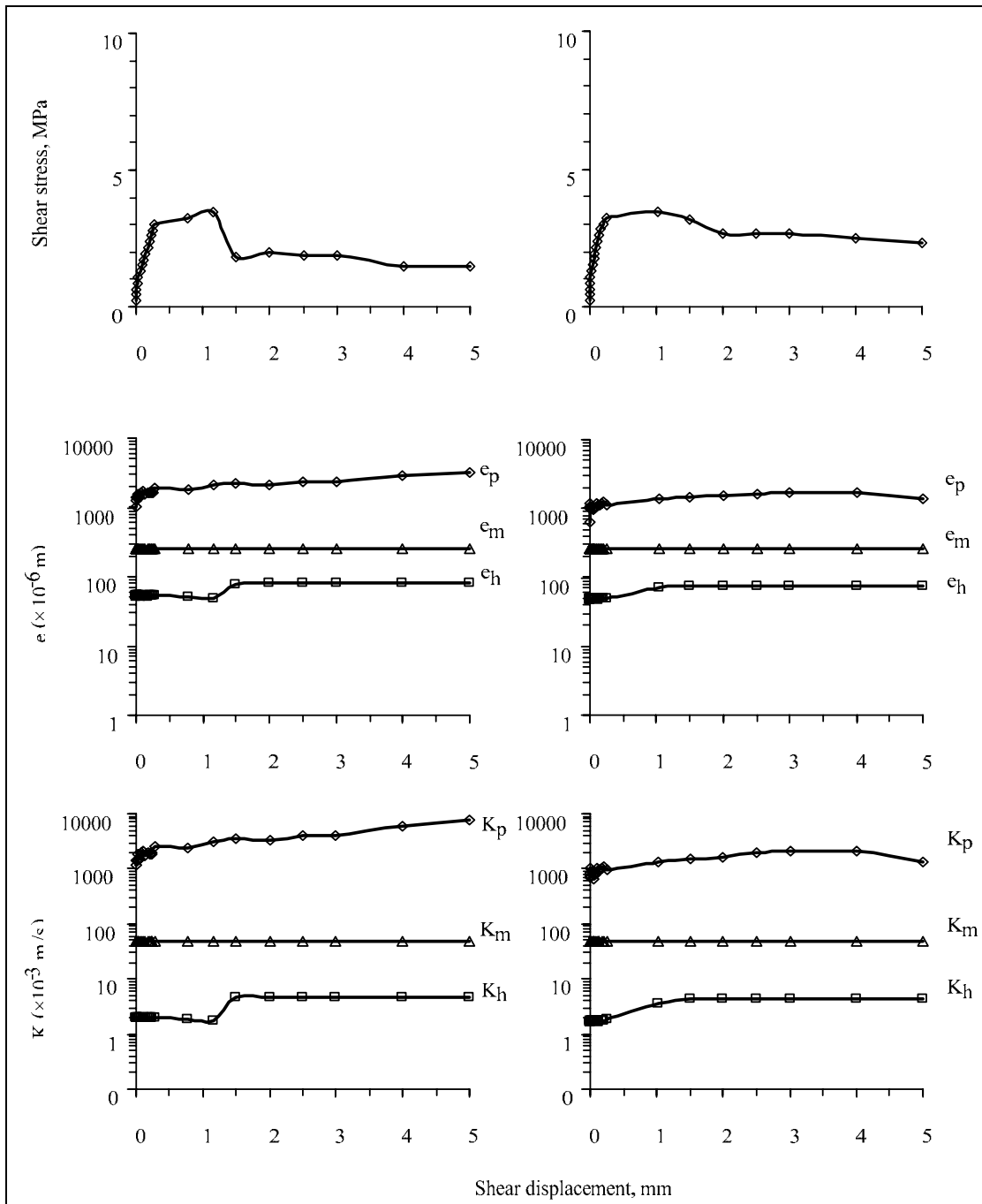
and 1.03 MPa (right) for Vietnamese granite.

Figure 4.10 Shear stress, fracture aperture, and hydraulic conductivity as a function

of shear displacement (δ_s) at normal stress = 2.07 MPa (left)

and 3.10 MPa (right) for Vietnamese granite.

4.4 Effect of normal stresses

The fracture permeability values under no shear stress, immediately before the peak stress, and under the residual shear stress are compared. The fracture permeability under residual shear region is higher than that under no shear and before peak stress. The magnitudes of fracture permeability under no shear and under peak stress are similar.

Both tend to decrease exponentially with the normal stress. Figure 4.11 plotted the equivalent hydraulic aperture e_h and the hydraulic conductivity K_h as a function of normal stress σ_n. As a result the difference between the permeability under residual shear stress and that under peak stress becomes larger as the normal stress increases. The results agree reasonably well with those obtained by Lee and Cho (2002); Son et al. (2004).

4.5 Effect of shear strength

Figures 4.12 and 4.13 plot the fracture hydraulic conductivity, K_h as a function of fractures shear strength. The fracture hydraulic conductivity decreases with increasing fracture shear strength. The decrease of the K_h with the peak shear strength can be represented by an exponential equation:

$$K_h = \alpha_p \exp (\beta_p \tau_p) \qquad (4.6)$$

where α_p is empirical constant and β_p is empirical constants.

For the residual shear strength the change of K_h can be represented by

$$K_h = \alpha_r \exp(\beta_r \tau_r) \tag{4.7}$$

where α_r is empirical constant and β_r is empirical constants.

The exponent β_p and β_r represent the reduction rate of the fracture permeability as the fracture shear strength increases. The hydraulic conductivity determined under peak strength tends to decrease more rapid than that determined under residual strength. Table 4.2 summarizes the results.

Table 4.2 Summary of the empirical constants α and β for all rock types.

Rock Samples	α_p	α_r	β_p	β_r
SMB	22.160	29.016	-0.488	-0.214
TGR	31.355	30.372	-0.355	-0.640
CGR	25.589	23.663	-0.470	-0.001
VGR	15.107	25.449	-0.126	-0.202

4.6 Permeability as a function of shear and normal stress

Empirical equations are developed to determine from hydraulic conductivity (determined from hydraulic aperture) under the corresponding normal and shear stresses, hydraulic aperture and joint displacement. They are developed from residual strength parameters because the behavior of hydraulic conductivity before peak shear strength are negligible. Figures 4.14 and 4.15 plot the shear stress as a function of hydraulic conductivity and joint displacement ratio for various the normal stresses, which can be represented by a power equation.

Their empirical constants A_0 and B_0 depend on the normal stresses. A power equation can be used to correlate A_0 and B_0 with the normal stress (σ_n). The normalized hydraulic conductivity can be expressed as;

$$K_h = 10^{[(\log \tau - \log A_0)/B_0] + \log \delta} \qquad (4.8)$$

Similar to the derivation above, empirical relation can be developed for Tak granite, Vietnamese granite and Chinese granite. Table 4.3 summarizes the regression results of the constant A_0 and B_0. The above equation can therefore be used to predict the hydraulic conductivity of joint under any normal and shear stresses in the in-situ condition.

Table 4.3 Summary of the results of empirical constants A_0 and B_0 for all rock types.

Rock Samples	A_0	B_0
SMB	$1.31\sigma_n^{0.82}$	$0.12\sigma_n^{-0.43}$
TGR	$1.14\sigma_n^{0.68}$	$0.18\sigma_n^{-0.28}$
CGR	$1.09\sigma_n^{0.87}$	$0.16\sigma_n^{0.20}$
VGR	$0.96\sigma_n^{0.76}$	$0.33\sigma_n^{-0.13}$
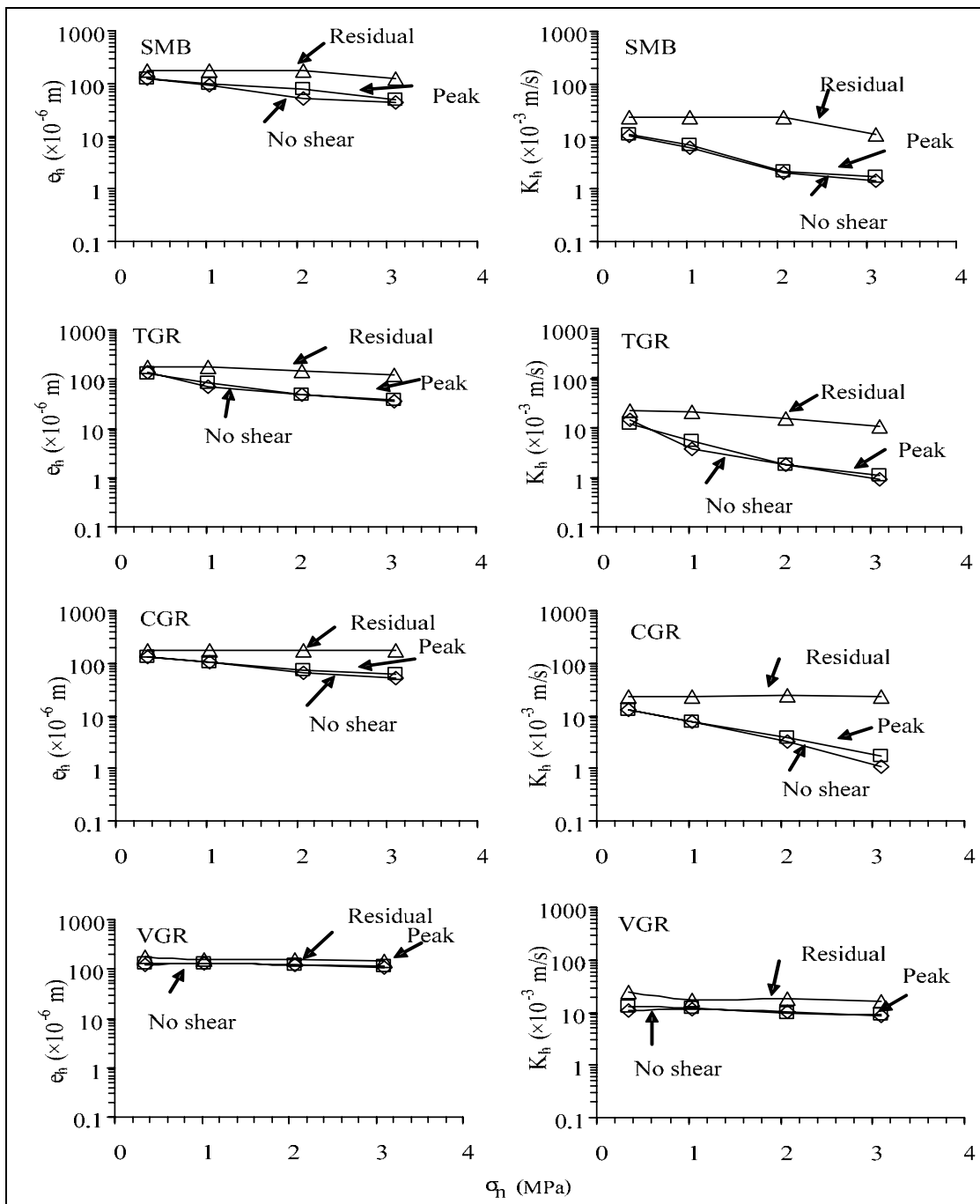
Figure 4.11 Hydraulic aperture (e_h) and hydraulic conductivity (determined from e_h)

as a function of normal stress (σ_n) for SMB, TGR, CGR and VGR.
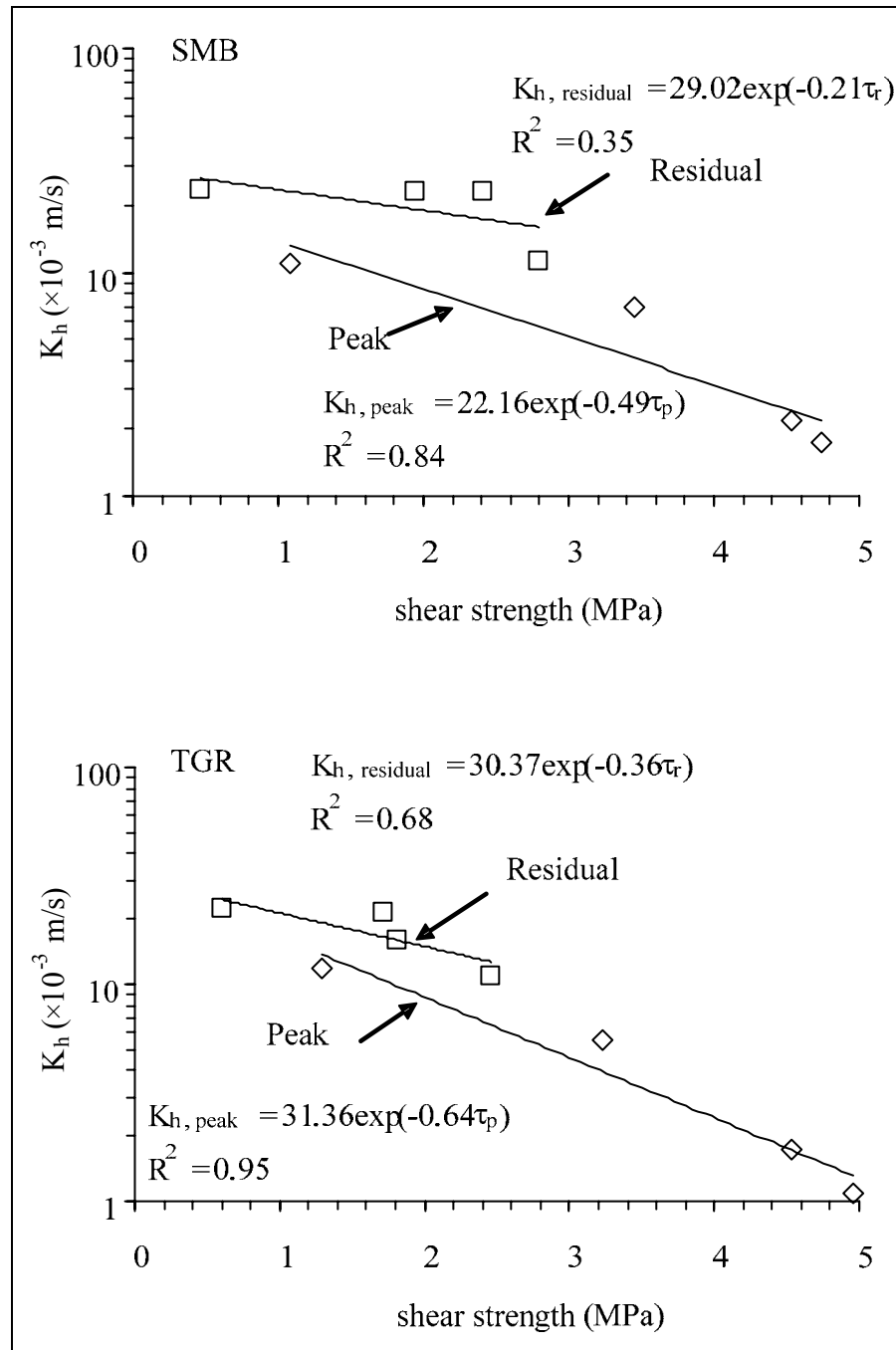
Figure 4.12 Hydraulic conductivity (K_h) as a function of peak and residual

shear strength for SMB and TGR.
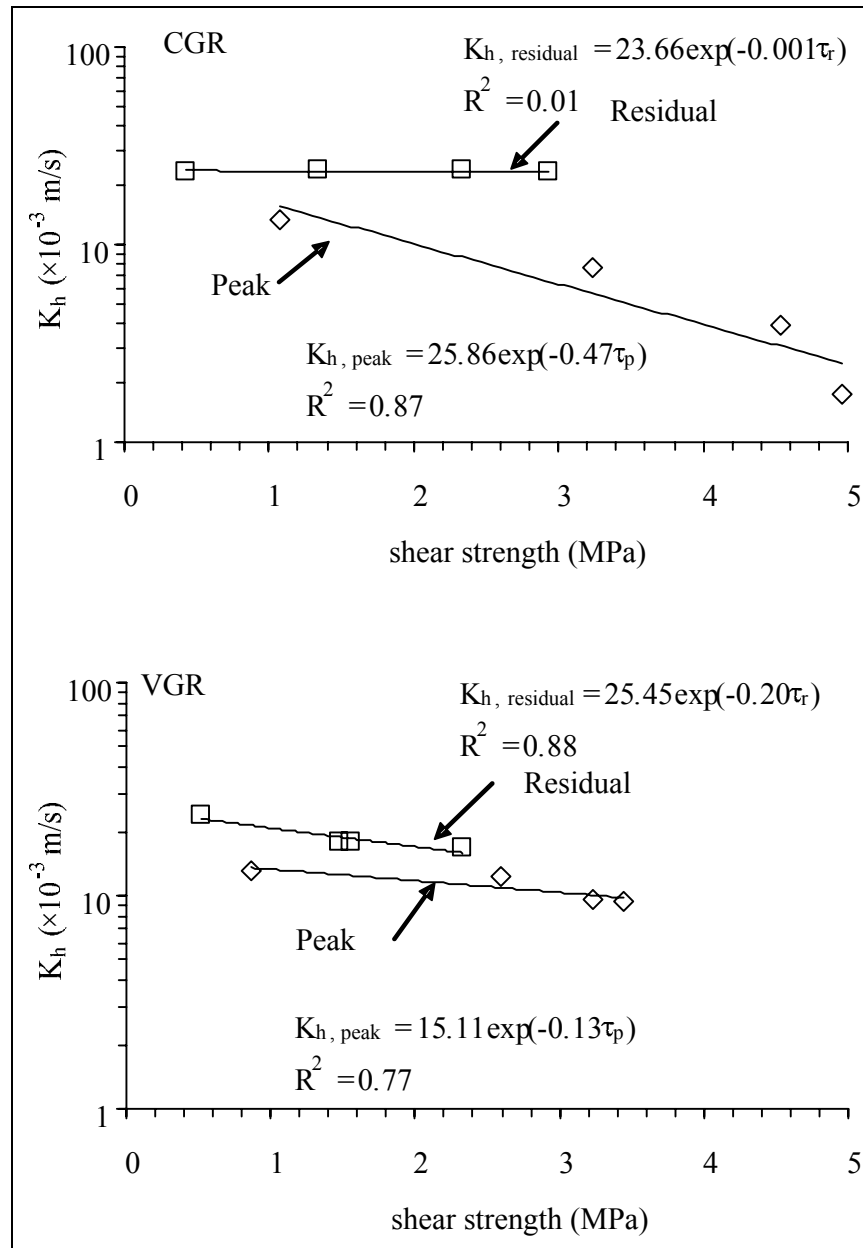
Figure 4.13 Hydraulic conductivity (K_h) as a function of peak and

residual shear strength for CGR and VGR.
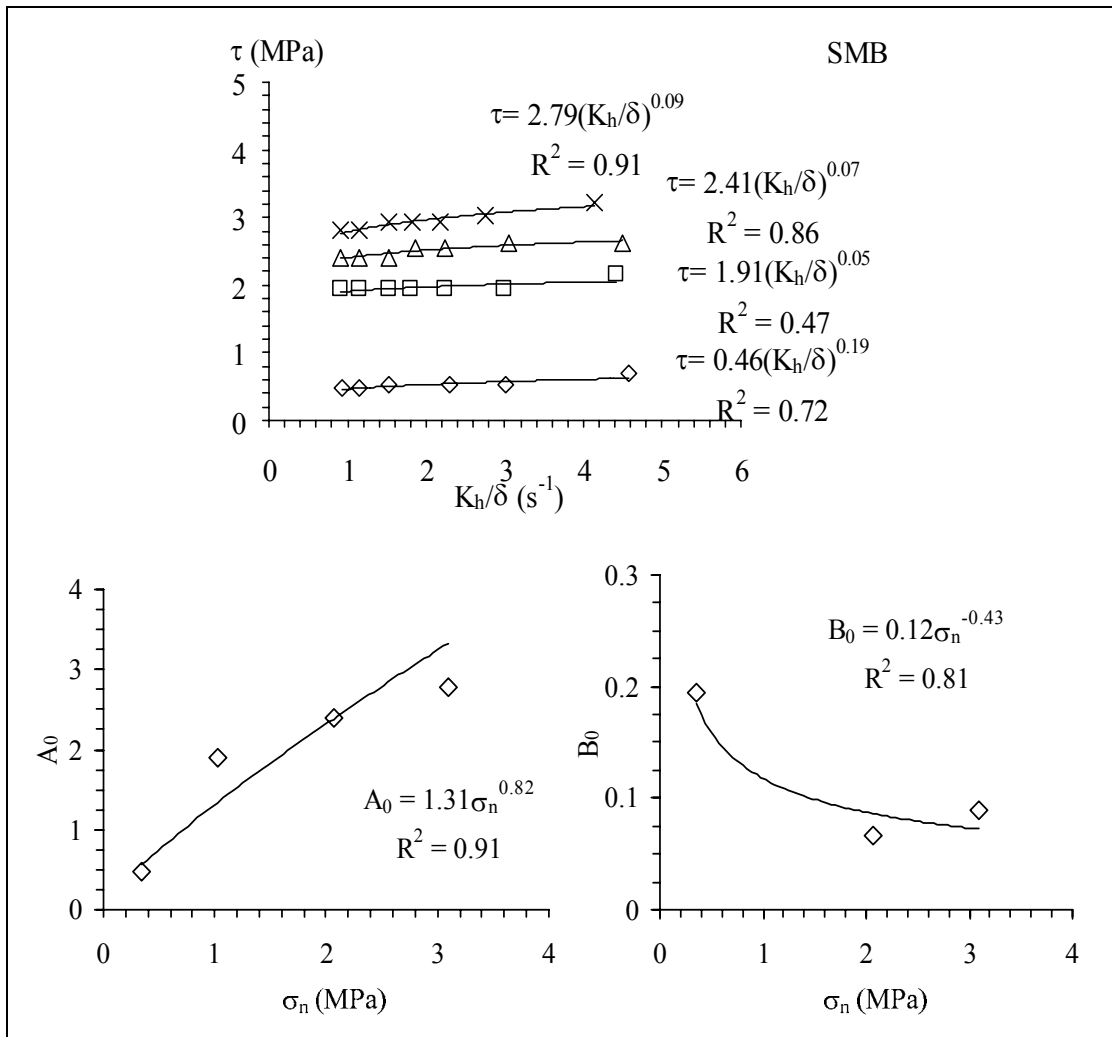
Figure 4.14 Relationship between shear stress as a function of hydraulic conductivity

and joint displacement ratio for various the normal stresses (top)

and empirical constants A_0 and B_0 (bottom) for SMB.
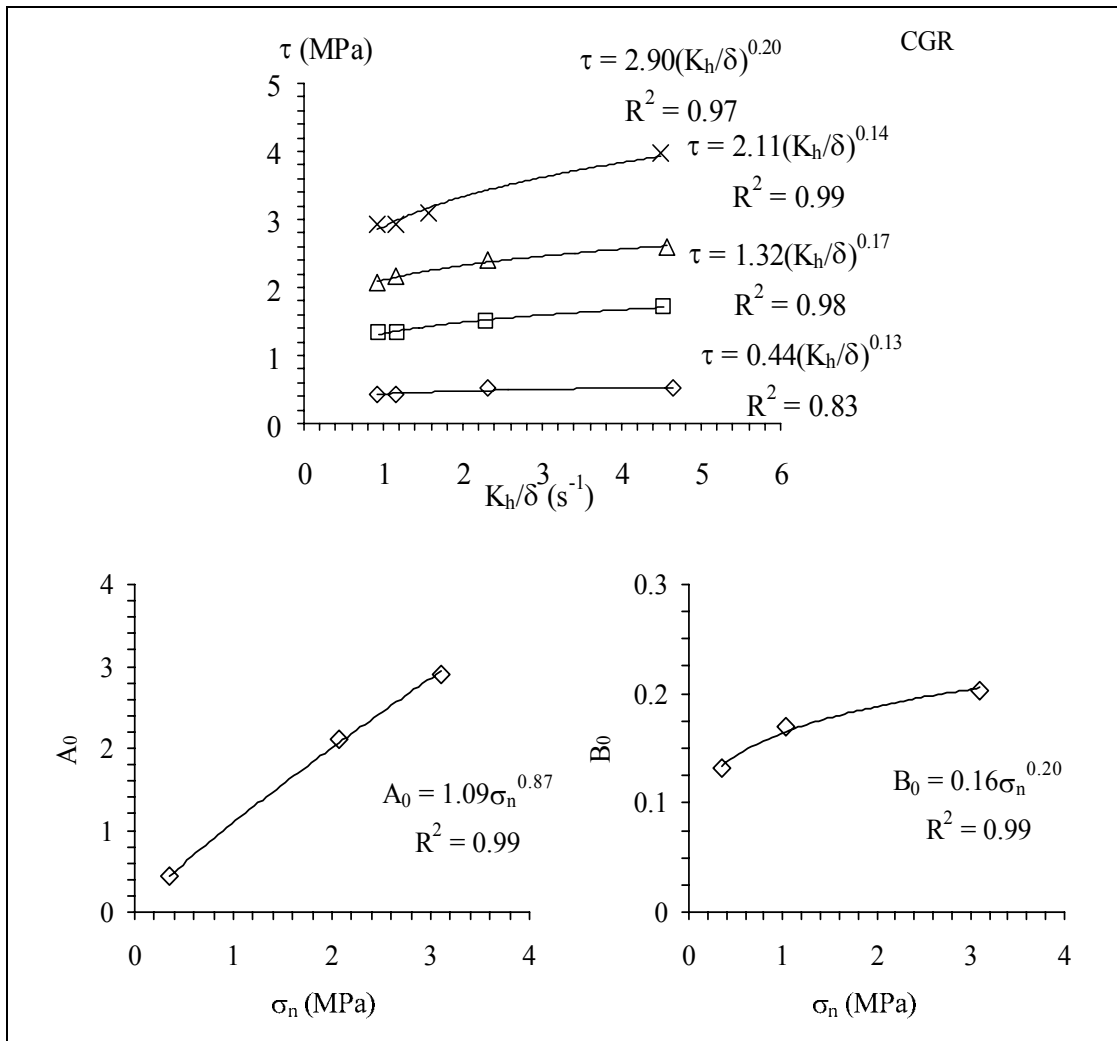
Figure 4.15 Relationship between shear stress as a function of hydraulic conductivity

and joint displacement ratio for various the normal stresses (top)

and empirical constants A_0 and B_0 (bottom) for CGR.
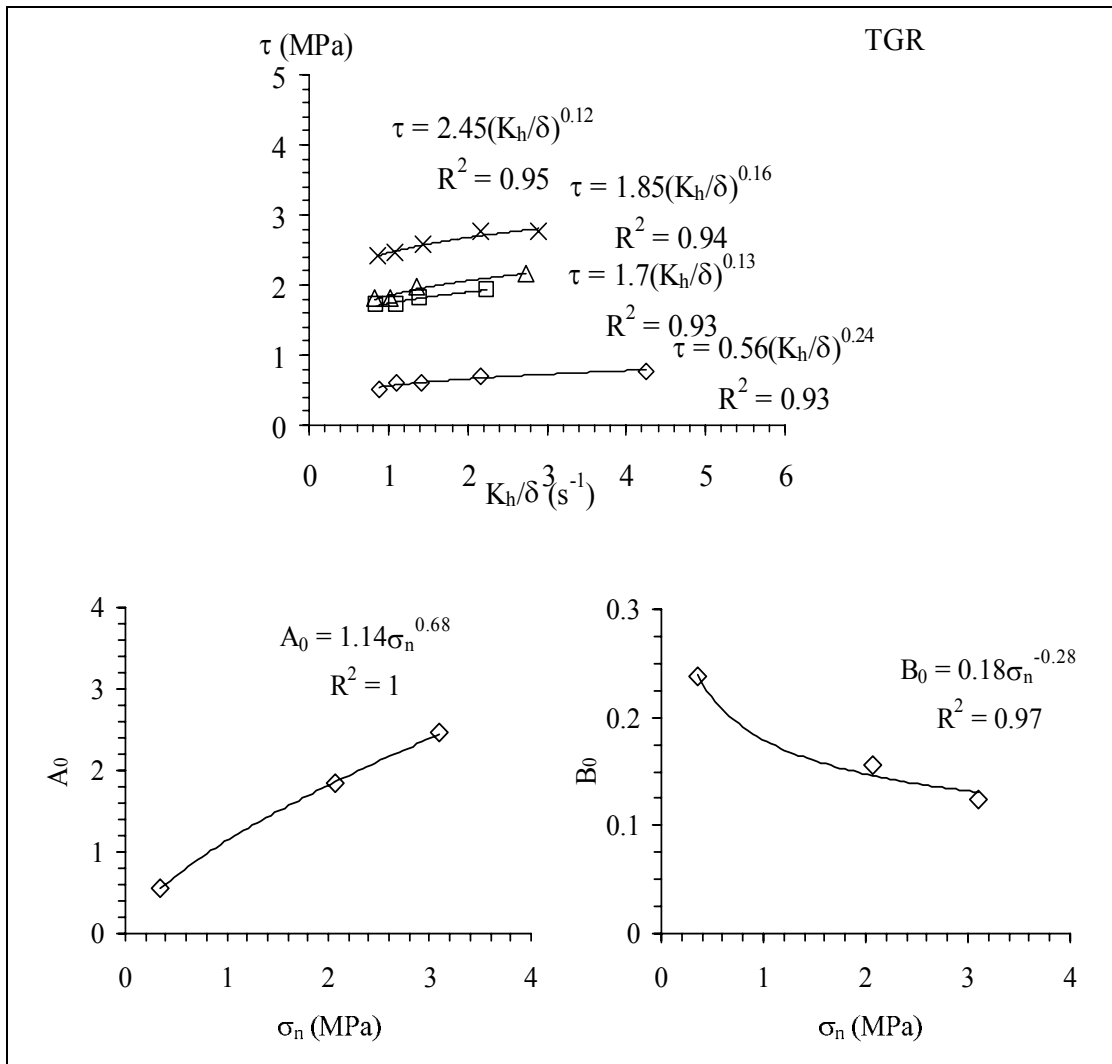
Figure 4.16 Relationship between shear stress as a function of hydraulic conductivity

and joint displacement ratio for various the normal stresses (top)

and empirical constants A_0 and B_0 (bottom) for TGR.
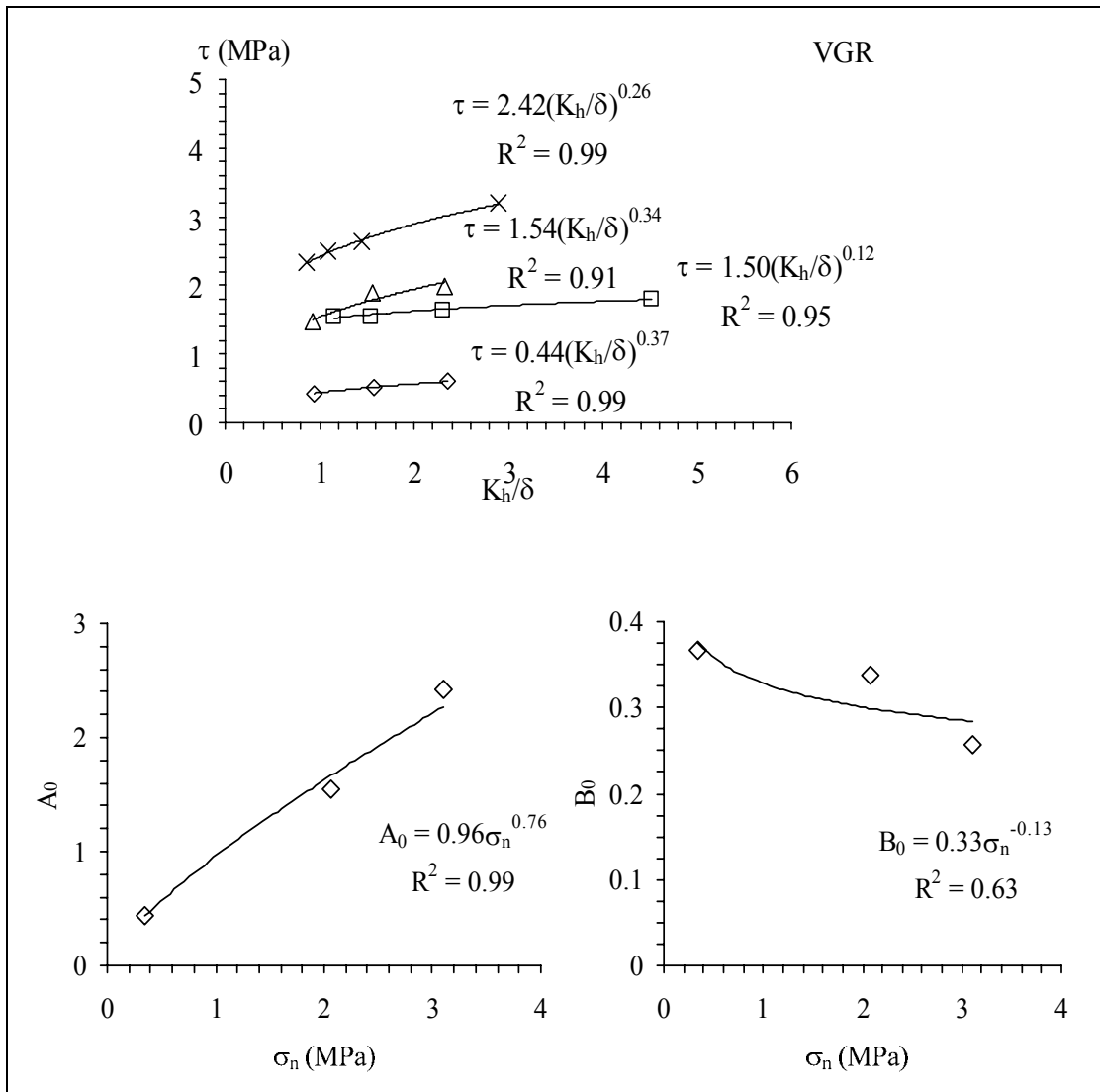
Figure 4.17 Relationship between shear stress as a function of hydraulic conductivity

and joint displacement ratio for various the normal stresses (top)

and empirical constants A_0 and B_0 (bottom) for VGR.

CHAPTER V

NUMERICAL MODELING

5.1 Introduction

This chapter describes the discrete element analysis using UDEC (Itasca, 2004) to study the permeability increase of fractured rock mass due to movements of rock blocks around excavations. The analysis determines the increase of joint displacements around underground excavations. Results from the mechanical deformation analysis are used in the evaluation of the changes of rock permeability as affected by the applied stresses. Property from Saraburi marble is used in the numerical modeling.

## 5.2 Rock properties for computer modeling

Before performing the computer analysis, physical and mechanical properties of rock samples are specified in the calculation. The major and significant constants in the models are friction angle, cohesion, normal stiffness and shear stiffness of the rock joints. They are obtained from the falling head test in the direct shear test. Table 5.1 gives summary of the parameters used in numerical simulation.

Table 5.1 Summary of the basic mechanical properties.

Basic mechanical properties	Saraburi marble
Peak friction angle (Degrees)	51
Residual friction angle (Degrees)	46
Cohesion (MPa)	1.42
Normal stiffness (GPa/m)	4.52 ± 2.19
Shear stiffness (GPa/m)	9.62 ± 6.23
Density (g/cc)	2.75

5.3 Discrete element analysis

The difficulty in predicting the underground excavation is due to the complexity of the post failure behavior of the rock mass and movement of the joint system. To demonstrate these issues discrete element analyses are performed using UDEC (Itasca, 2004) to simulate the movement of the jointed rock mass above a rectangular underground excavation. The discrete element models are constructed to represent a joint deformation around underground excavations. The excavation depth, width and height are maintained constant at 5 m, 10 m and 10 m, shown in Figure 5.1. A hydrostatic stress is applied on both sides of the model. There are two mutually perpendicular joint sets inclined at 45° and joint spacing for both cases is 1.8 m.

Different patterns of block arrangement can be obtained before and after excavating. Simulation results before excavation show that the joint displacement decreases when the depth increases. There is weight of the overburden. In the excavated condition, the failure occurs around the zone of excavation. As a result the difference between the stress and joint displacement can be used to determine the hydraulic conductivity obtains before and after excavation using equation 4.8 in Chapter 4. Figures 5.2 and 5.3 show contour lines of permeability computed from equation 4.8.
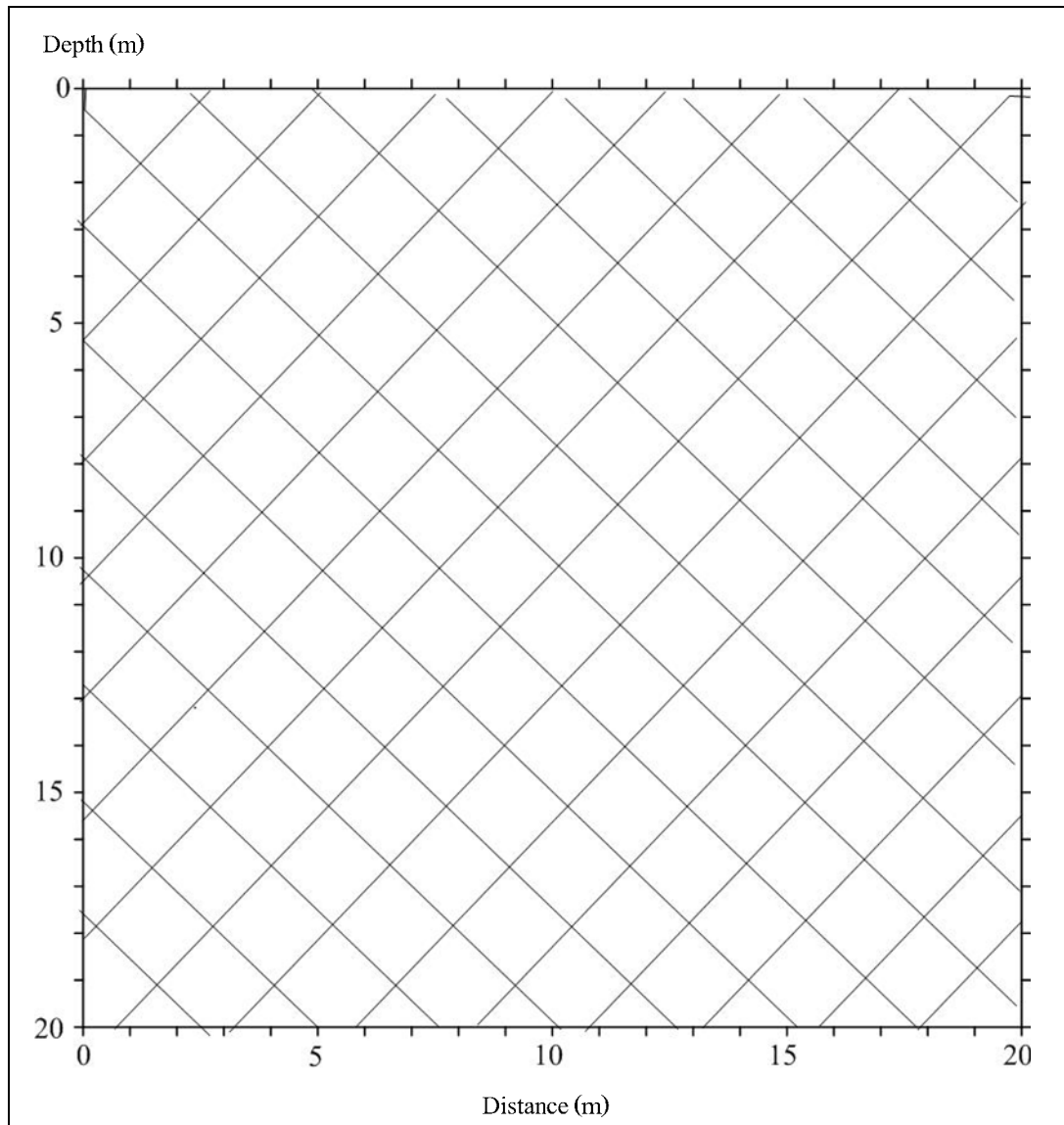
Figure 5.1 UDEC model: two mutually perpendicular joint sets inclined at 45°

and joint spacing for both cases is 1.8 m.
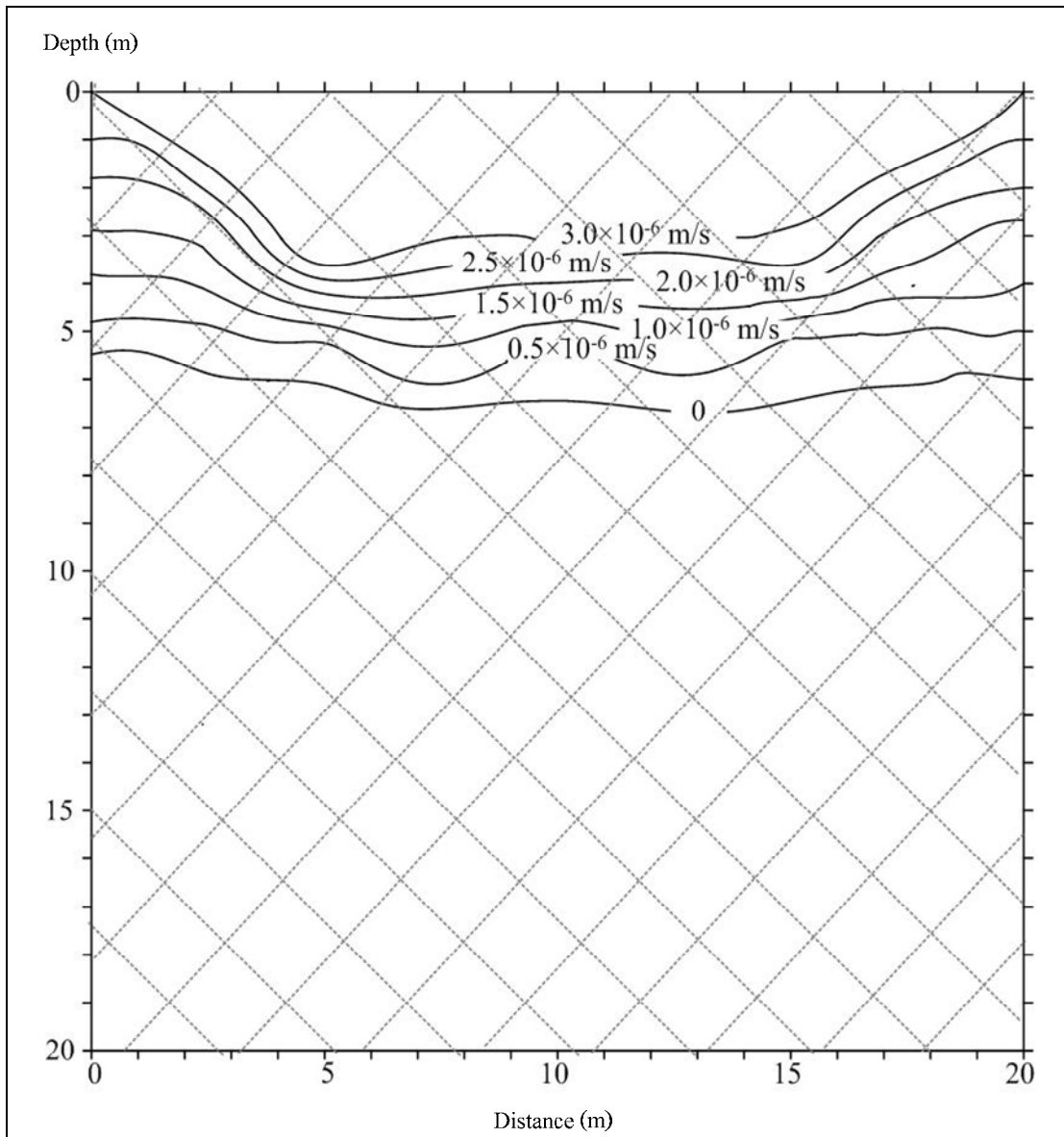
Figure 5.2 Permeability contours before excavation for Saraburi marble.
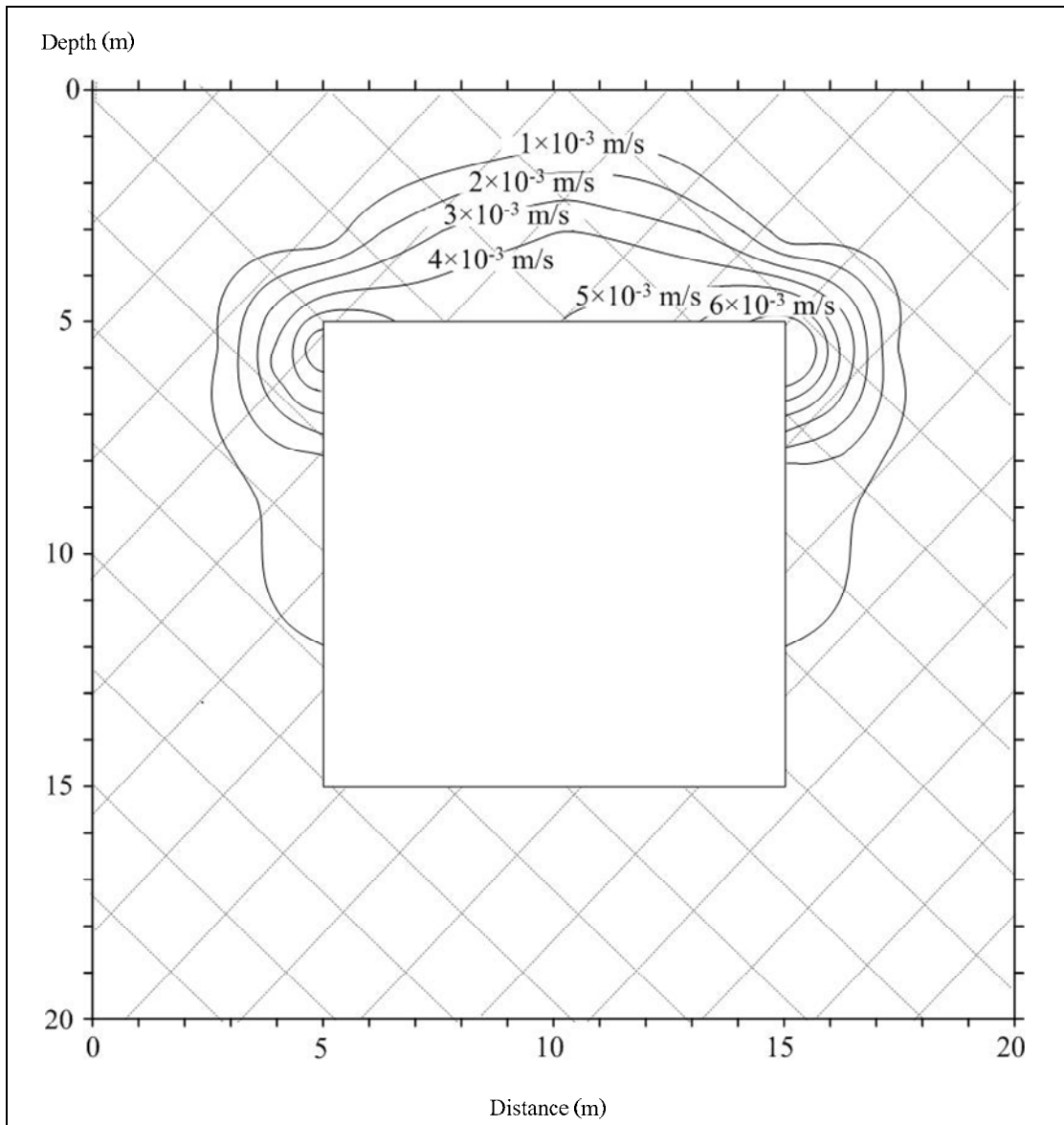
Figure 5.3 Permeability contours after excavation for Saraburi marble.

CHAPTER VI

DISCUSSIONS AND CONCLUSIONS

6.1   Discussions and conclusions

The physical aperture e_p and hydraulic aperture e_h increase with shearing displacement, particularly under high normal stresses. The magnitudes of fracture permeability under no shear and under peak shear stress are similar. For both peak and residual regions, the physical apertures are about 5 to 10 times greater than the hydraulic apertures, as a result the fracture hydraulic conductivity determined from the physical aperture are about one to two orders of magnitudes greater than these determined from the equivalent hydraulic apertures. These conclusions agree well with those of Suanprom et al. (2009).

The difference between the permeability under residual shear stress and that under peak stress becomes larger under higher normal stresses. The fracture hydraulic conductivities exponentially decrease with increasing the normal stresses. Their permeability is in the range between 1×10^{-3} m/s and 15×10^{-3} m/s. The fracture hydraulic conductivity determined here compares well with those obtained by Zhao (1998); Chandra et al. (2008).

The flow in fractures is sensitive to normal stiffness of discontinuity. The normal stiffness however tends to increase with increasing stress. In this research, the range of normal stiffness is approximately from 1 to 18 GPa/m which is of the same order of magnitude with those obtained by Pyrak-Nolte et al. (2000).

The difficulty in predicting the underground excavation is due to the complexity of the post failure behavior of the rock mass and movement of the joint system. To demonstrate these issues discrete element analyses are performed using UDEC (Itasca, 2004) to simulate the movement of the jointed rock mass above a rectangular underground excavation. Different patterns of block arrangement can be obtained before and after excavating. Simulation results before excavation show that the joint displacement decreases when the depth increases. There is weight of the overburden. Under the excavated condition, the failure occurs around the zone of excavation, and results in an increase of the rock joints.

6.2 Recommendations for future studies

The study in this research can be taken as a preliminary guideline and process of study and design. The fracture area should be larger. The fracture permeability should be obtained from shearing specimen while the dilation is maintained constant. The hydraulic head should be applied at different levels and maybe using gas as flow medium.

REFFERENCES

Akkrachattrarat, N., Suanprom, P., Buaboocha, J., and Fuenkajorn, K. (2009). Flow testing of sandstone fractures under normal and shear stresses. **Proceeding of The Second Thailand Symposium on Rock Mechanics** , Chonburi, Thailand, pp. 319-334.

Auradou, A., Drazer, G., Boschan, A., Hulin, J.P., and Koplik, J. (2006). Flow channeling in a single fracture induced by shear displacement. **Geothermics**. 35(5-6) : 576–588.

Baghbanan, A., and Jing, L. (2006). Hydraulic properties of fractured rock masses with correlated fracture length and aperture. **International Journal of Rock Mechanics & Mining Sciences.** 44 (5) : 704–719.

Baghbanan, A., and Jing, L. (2008). Stress effects on permeability in a fractured rock mass with correlated fracture length and aperture. **International Journal of Rock Mechanics & Mining Sciences**. 45(8) : 1320-1334.

Bandis, S.C., Barton, N.R., and Christianson, M. (1985). Application of a new numerical model of joint behavior to rock mechanics problems. **In Proceeding of the International Symposium on Fundamentals of Rock Joints**, Bjorkliden.

Bandis, S.C., Lumsden, A.C., and Barton, N.R. (1983). Fundamentals of rock joint deformation. **International Journal of Rock Mechanics and Mining Sciences & Geomechanics Abstracts**. 20(6):249-268.

Barton, N. (1973). Review of a new shear-strength criterion for rock joints. **Engineering Geology**. 7(4):287-332.

Barton, N., and Bakhtar, K. (1983). **Rock Joint Description and Modeling of the Hydrothermomechanical Design of Nuclear Waste Repositories (Contact Report, Submitted to CANMET)**. Mining Research Laboratory, Ottawa.

Chandra, S., Ahmed, S., Ram, A., and Dewandel, B. (2008). Estimation of hard rock aquifers hydraulic conductivity from geoelectrical measurements : A theoretical development with field application. **Journal of Hydrology.** 357 (3-4) : 218-227.

Giacominia, A., Buzzib, O., Ferreroa, A.M., Migliazzaa, M., and Giania, G.P. (2008). Numerical study of flow anisotropy within a single natural rock joint. **International Journal of Rock Mechanics & Mining Sciences**, 45 (1) : 47–58.

Hamiel, Y., Lyakhovsky, V., and Agnon, A. (2005). Rock dilation, nonlinear deformation, and pore pressure change under shear. **A Institute of Earth Sciences, Hebrew University of Jerusalem**.

Hans, J. (2002). Etude expérimentale et modélisation numérique multiéchelle du comportement hydromécanique des répliques de joints rocheux. **PhD thesis, Joseph Fourier University, Grenoble, France, 2002**.

Indraratna, B., and Ranjith, P. (2001). Hydromechanical aspects and unsaturated flow in joints rock. **Lisse : A. A. Balkema**.

Itasca (2004). **UDEC 4.0 GUI A Graphical User Interface for UDEC**. Itasca Consulting Group Inc., Minneapolis, Minnesota.

Jiang, Y., Tanabashi, Y., Xiao, J., and Nagaie (2004). An improved shear-flow test apparatus and its application to deep underground construction. Paper 1A 28 - SINOROCK2004 Symposium. **Internationa Journal of Rock Mechanics and Mining Sciences**. Vol. 41, No. 3, CD-ROM.

Kemthong, R., and Fuenkajorn, K. (2007). Prediction of joint shear strenghs of ten rock types using field-identified parameters. **Rock Mechanics Proceedings of First Thailand Symposium,** Nakhon Ratchasima, Thailand, pp. 195-209.

Lee, H.S., and Cho, T.F. (2002). Hydraulic characteristics of rough fractures in linear flow under normal and shear load. **Rock Mechanics and Rock Engineering**. Springer-Verlag Wien. 35(4):299-318.

Maini, Y.N.T. (1971). In situ hydraulic parameters in jointed rock-their measurement and interpretation. **Ph.D. Thesis. Imperial College, London**. 321 p.

National Research Council. (1996). **Rock Fractures and Fluid Flow: Contemporary Understanding and Applications**. Washington, D.C.: National Academy Press.

Pyrak-Noltea, L.J., and Morrisa, J.P. (2000). Single fractures under normal stress: The relation between fracture specific stiffness and fluid flow. **International Journal of Rock Mechanics and Mining Sciences.** 37(1):245-262.

Son, B.K., Lee, Y.K., and Lee, C.I. (2004). Elasto-plastic simulation of a direct shear test on rough rock joints. **International Journal of Rock Mechanics & Mining Sciences**. 41(3):1-6.

Suanprom, P., Obcheoy, J., and Fuenkajorn, K. (2009). Permeability of rock fractures under shear stresses. **EIT-JSCE Joint International Symposium Geotechnical Infrastructure Asset Management,** Bangkok, Thailand.

Terzaghi, K. (1936). The Shearing Resistance of Saturated Soils. pp.402-407. **Proceedings of the International Conference on Foundation Engineering**, Graduate School of Engineering, Harvard University. Boston: Spaulding Moss Co.

Zeigler, B. (1976). **Theory of Modelling and Simulation**. New York: John Wiley and Sons.

Zhao, J. (1998). Rock mass hydraulic conductivity of the Bukit Timah granite, Singapore. **Engineering Geology**. 50(1-2) : 211-216.

APPENDIX A

SHEAR STRESS-DISPLACEMENT CURVES

FROM DIRECT SHEAR TESTS
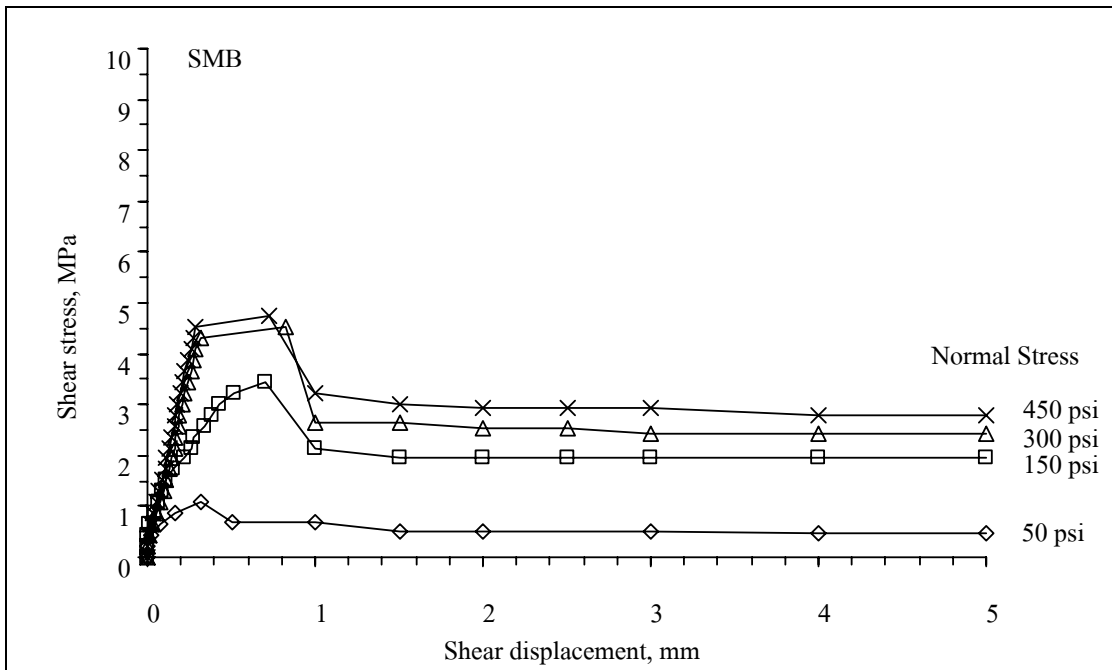
Figure A.1 Shear stress as a function of shear displacement for SMB.
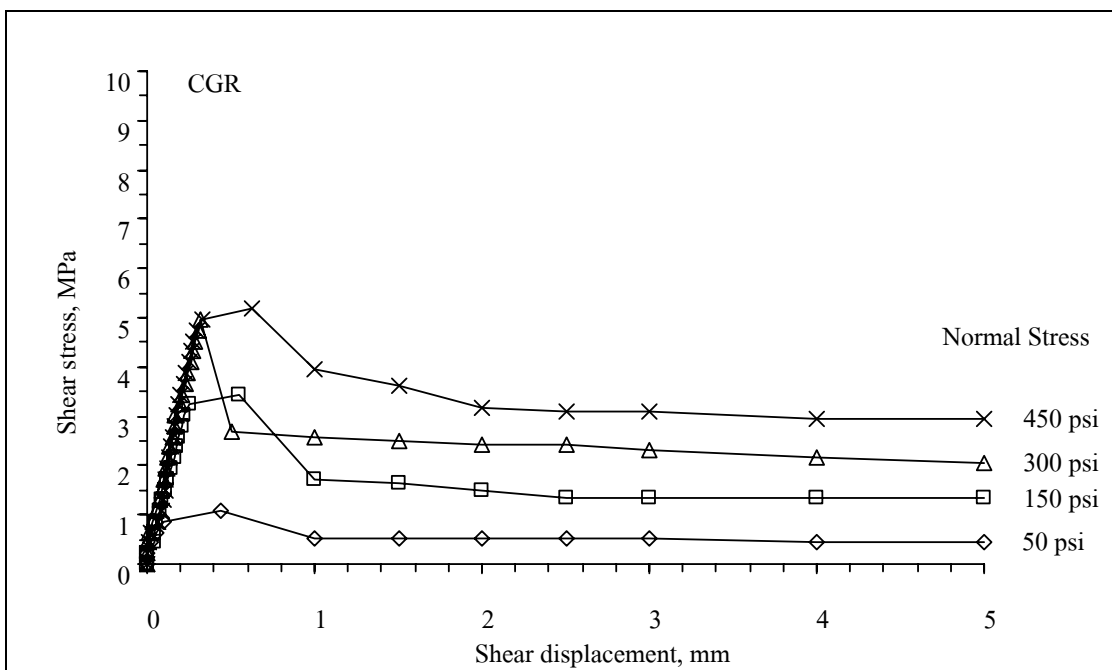
Figure A.2 Shear stress as a function of shear displacement for CGR.
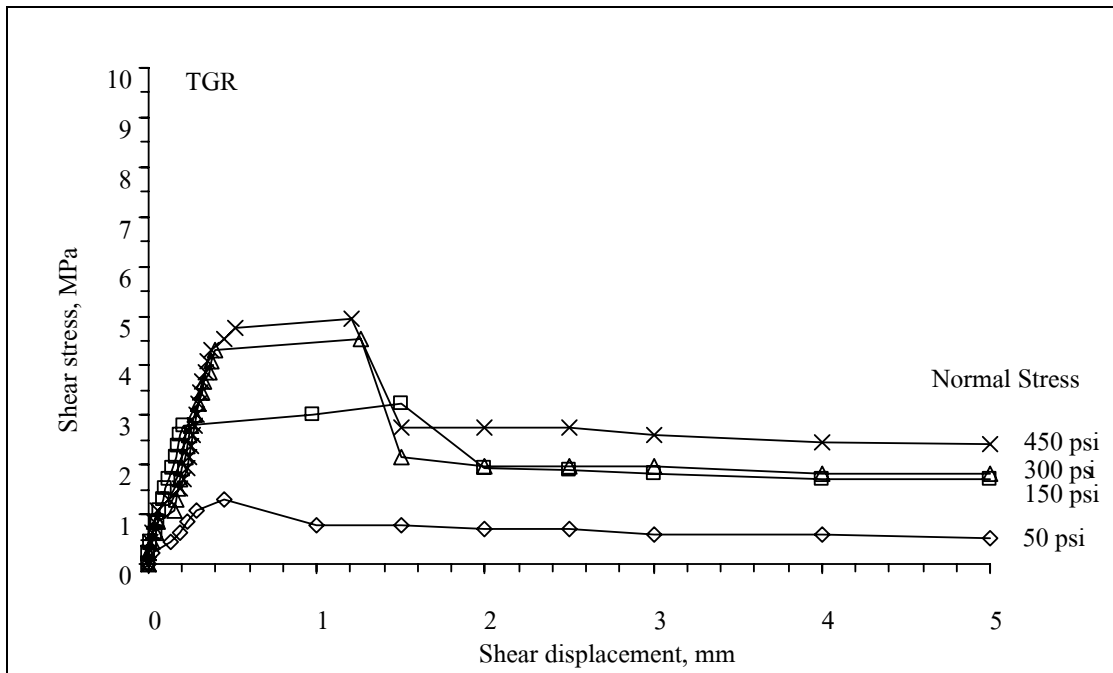
Figure A.3 Shear stress as a function of shear displacement for TGR.
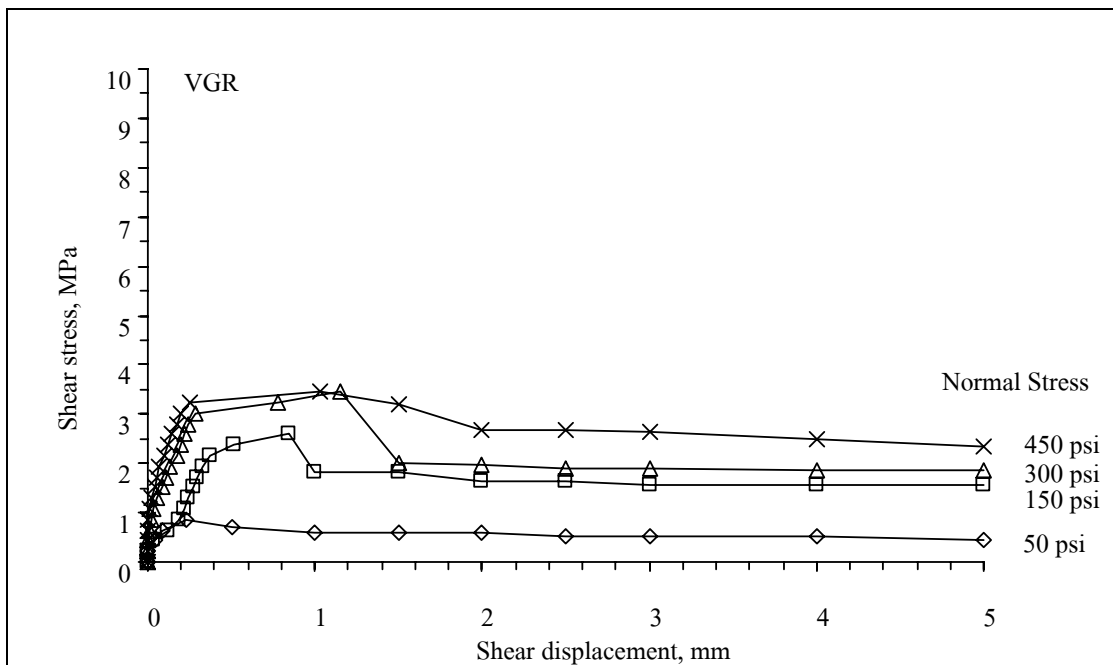
Figure A.4 Shear stress as a function of shear displacement for VGR.

APPENDIX B

TECHNICAL PUBLICATION

TECHNICAL PUBLICATION

Obcheoy, J., Aracheeploha, S., and Fuenkajorn, K. (2011). **Fracture Permeability under normal and shear stresses.** Thailand Rock Mechanics Symposium. Phetchaburi, Thailand, 10-11 March 2011.

Fracture permeability under normal and shear stresses

J. Obcheoy, S. Aracheeploha & K. Fuenkajorn
Geomechanics Research Unit, Suranaree University of Technology, Thailand

ABSTRACTS: Flow tests have been performed to determine hydraulic conductivity of tension-induced fractures under normal and shear stresses. The fractures in four rock types have been tested: Saraburi marble, Tak granite, Vietnamese granite and Chinese granite. The results indicate that the physical aperture e_p and hydraulic aperture e_h increase with shearing displacement, particularly under high normal stresses. The magnitudes of fracture permeability under no shear and under peak shear stress are similar. For both peak and residual regions, the physical apertures are about 5 to 10 times greater than the hydraulic apertures, as a result the fracture hydraulic conductivity determined from the physical aperture are about one to two orders of magnitudes greater than these determined from the equivalent hydraulic apertures. This is probably because the measured physical apertures do not consider the effect of fracture roughness that causes a longer flow path. The difference between the permeability under residual shear stress and that under peak stress becomes larger under higher normal stresses. The fracture hydraulic conductivities exponentially decrease with increasing the normal stresses. Their permeability is in the range between 1.0×10^{-3} m/s and 15×10^{-3} m/s.

1   INTRODUCTION

Groundwater in rock mass is one of the key factors governing the mechanical stability of slope embankments, underground mines and tunnels. Permeability of rock mass is path dependent, controlling mainly by the system of fractures as the permeability of most intact rocks is significantly lower. For undisturbed rock mass (before excavation) the joint characteristics that dictate the amount and direction of water flow, can be adequately determined by means of in-situ measurements, and sometimes assisted by numerical modeling. Slope or underground excavations disturb the surrounding rock mass, alter the stress states on the fracture planes, and often cause relative displacements of the fractures. The excavations usually increase the surrounding rock mass permeability, sometimes by several orders of magnitudes. Even though this effect has long been recognized, study on the rock fracture permeability as affected by the shearing displacement has been rare.

Fracture permeability under normal and shear stresses

The objective of this research is to experimentally assess the permeability of rock fractures under shearing displacements. The effort involves performing a series falling head tests on tension-induced fractures in four rock types, including Saraburi marble, Tak granite, Vietnamese granite and Chinese granite. The changes of the physical and hydraulic apertures, the water flow rates, and the applied shear stresses are monitored and used to calculate the changes of the fracture permeability as a function of shear displacement. Empirical relations are developed to determine the fracture permeability as a function of the stresses and fracture displacement.

2   ROCK SAMPLES

The tested rocks are Saraburi marble, Tak granite, Vietnamese granite and Chinese granite. Four specimens are tested for each rock type. Samples for the falling head test are prepared to have fractures area of about 10×10 cm^2. The fractures are artificially made in the laboratory by tension inducing method. Figure 1 shows rock fracture induced in the four rock types.

3   TEST METHOD

Falling head tests are conducted by injecting water into the center hole of rectangular blocks of the specimen. The laboratory arrangement of the falling head flow test while the fracture is under normal and shear stresses is shown in Figure 2. The maximum water head above the tested fracture is 1.23 m. The injection hole at the center of the lower block is 0.8 cm in diameter. The fractures are artificially made by applying a line load to induce a splitting tensile crack in $10 \times 10 \times 7.6$ cm prismatic blocks of rocks samples. The fracture area is 10×10 cm. Their roughness is observed and classified by comparing with a reference profiles given by Barton (joint roughness coefficient – JRC, Barton, 1973). The constant normal stresses are 0.35, 1.03, 2.07 and 3.10. MPa. The shear stress is applied while the shear displacement and head drop are monitored for every 0.5 mm of shear displacement. The maximum shear displacement is 10 mm. The (physical) fracture aperture is measured to the nearest 0.01 mm before and after normal and shear stress application. The fracture dilations are also monitored during the shear test.

The physical, mechanical and hydraulic apertures are used to calculate the hydraulic conductivity of the tested fractures. The physical aperture (e_p) is obtained from the actual measurements of the fractures before and during normal and shear stress applications. The measurement points are at the four corners of the shear box. The physical aperture at each shear displacement is an average from the four measurements. The mechanical aperture (e_m) in mm is calculated by (Barton & Bakhtar, 1983; Bandis et al., 1983, 1985):
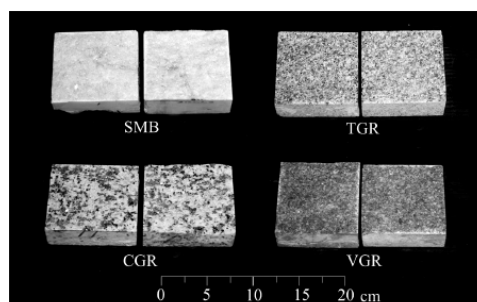
Figure 1. Some rock specimens prepared for falling head
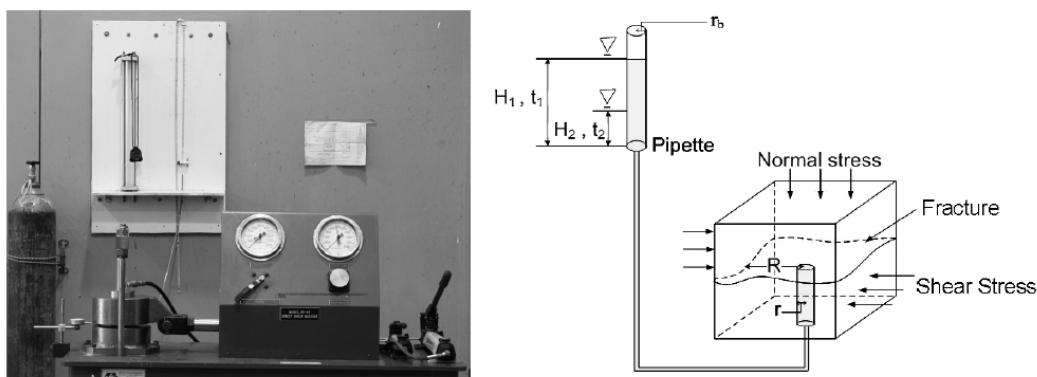
Figure 2. Laboratory arrangement for falling head flow tests while the rock specimen is in the direct shear device.

$$e_m = [JRC/5] / [0.2(\sigma_c/JCS) - 0.1] \qquad (1)$$

where σ_c is the uniaxial compressive strength of the rock (MPa), JCS is joint compressive strength of the rock (MPa). Here σ_c and JCS are assumed to be equal. The measured JRC values range from 9, 11, 13 and 15. From equation (1) the equivalent mechanical apertures for the above JRC values are 180, 220, 260 and 300 micro-meters.

The equivalent hydraulic aperture (e_h) for radial flow is calculated by (Maini, 1971):

$$e_h = [[\ln(H_1 / H_2)r_b^2 \ln(R / r)6\mu] / [(t_2 - t_1)\gamma]]^{1/3} \qquad (2)$$

where γ is unit weight of water (N/m^2), μ is dynamic viscosity (N·s/m^2), H_1, H_2 is water heads at t_1 and t_2, r_b is pipette radius (m), R is radius of flow path (m), r is radius of the radius injection hole (m).

The fracture permeability is calculated by (Zeigler, 1976):

$$K = \gamma e^2 / 12\mu \qquad (3)$$

Where K is hydraulic conductivity between smooth and parallel plates, e is parallel plate aperture. It is assumed here that the flow is laminar and isotropic across the fracture plane, and that the intact rock is impermeable.

4 TEST RESULTS

Table 1 summarizes the results of the fracture stiffness calculations for Saraburi marble, Tak granite, Vietnamese granite and Chinese granite. The fracture stiffness determined here compare well with those obtained by Pyrak-Nolte et al (2000) and Suamprom et al (2009). The joint shear stiffness tends to increase with the normal stresses.

Table 1. Normal and shear stiffness of rock samples.

Rock Types	K_s (GPa/m)	K_n (GPa/m)
SMB	9.62 ± 6.23	4.52 ± 2.19
TGR	11.53 ± 5.71	4.47 ± 2.18
CGR	13.77 ± 4.83	2.37 ± 1.37
VGR	6.83 ± 1.76	3.21 ± 2.22

The fracture permeability is calculated from the equivalent hydraulic aperture (e_h) and from the physical aperture (e_p) for the peak ($K_{h, peak}$, $K_{p, peak}$) and residual ($K_{h, residual}$, $K_{p, residual}$) stresses. The mechanical aperture, e_m before, during and after shearing therefore remains constant for each fracture. As a result the hydraulic conductivity K_m calculated from e_m is independent of the shearing displacement.

The physical aperture e_p tends to increase with shearing displacement. Its value fluctuates before the peak and tends to be more consistent in the residual stress region. The K_p values calculated from e_p subsequently show similar characteristics of the curves in the permeability-shear displacement diagram.

The hydraulic aperture e_h indirectly determined from the inflow rates also tends to increase with the shear displacement, particularly under high normal stresses. Even though K_p and K_h show similar characteristics of the curves in the permeability-shear displacement diagram, K_p is always about an order of magnitude greater than K_h, particularly in the residual shear region.

5   EFFECT OF NORMAL STRESS

The fracture permeability under residual shear region is higher than that under no shear and before peak stress. The magnitudes of fracture permeability under no shear and under peak stress are similar. Both tend to decrease exponentially with the normal stress. Figure 3 plotted e_h and K_h as a function of σ_n. The difference between the permeability under residual shear stress and that under peak stress becomes larger as the normal stress increases. The results agree reasonably well with those obtained by Lee and Cho (2002) and Son et al. (2004).

6   EFFECT OF SHEAR STRESS ON FRACTURE

Figure 4 plots the fracture hydraulic conductivity, K_h as a function of fractures shear strength. The fracture hydraulic conductivity decreases with increasing fracture shear strength. The decrease of K_h with the peak shear strength can be represented by an exponential equation:

$$K_h = \alpha_p \exp (\beta_p \tau_p) \tag{4}$$

where α_p and β_p are empirical constants.

For the residual shear strength the change of K_h can be represented by

$$K_h = \alpha_r \exp (\beta_r \tau_r) \tag{5}$$

where α_r and β_r are empirical constants.

Figure 3. Hydraulic aperture (e_h) and hydraulic conductivity (determined from e_h) as a function of normal stress (σ_n) for SMB, TGR, CGR and VGR.

Fracture permeability under normal and shear stresses

Figure 4. Hydraulic conductivity (K_h) as a function of peak and residual shear strength.

The exponents β_p and β_r represent the reduction rate of the fracture permeability as the fracture shear strength increases. The hydraulic conductivity determined under peak strength tends to decrease more rapid than that determined under residual strength.

7 MATHEMATICAL RELATIONSHIPS

The empirical equations are developed to determine the hydraulic conductivity under the corresponding normal and shear stresses, hydraulic aperture and joint displacement. They are developed from residual strength parameters because the behavior of hydraulic conductivity before peak shear strength are negligible. Figure 5 plots the shear stress as a function of hydraulic conductivity and joint displacement ratio for various the normal stresses (for Saraburi marble), which can be represented by power equation.

Their empirical constants A_0 and B_0 depend on the normal stresses. A power equation can be used to correlate A_0 and B_0 with the normal stress (σ_n), as shown in Figure 5. The normalized hydraulic conductivity can be expressed as;

$$K_h = 10^{[(\log \tau - \log A_0)/B_0] + \log \delta} \tag{6}$$

Similar to the derivation above, empirical relation can be developed for Tak granite, Vietnamese granite and Chinese granite. Table 2 summarizes the results.

Figure 5. Shear stress as a function of hydraulic conductivity and joint displacement ratio for various normal stresses (top) and empirical constants A_0 and B_0 (bottom) for SMB.

Table 2. Summary of empirical constants A_0 and B_0.

Rock Samples	A_0	B_0
SMB	$1.31\sigma_n^{0.82}$	$0.12\sigma_n^{-0.43}$
TGR	$1.14\sigma_n^{0.68}$	$0.18\sigma_n^{-0.28}$
CGR	$1.09\sigma_n^{0.87}$	$0.16\sigma_n^{0.20}$
VGR	$0.96\sigma_n^{0.76}$	$0.33\sigma_n^{-0.13}$

8   DISCUSSIONS AND CONCLUSIONS

The physical aperture e_p and hydraulic aperture e_h increase with shearing displacement, particularly under high normal stresses. The magnitudes of fracture permeability under no shear and under peak shear stress are similar. For both peak and residual regions, the physical apertures are about 5 to 10 times greater than the hydraulic apertures, as a result the fracture hydraulic conductivity determined from the physical aperture are about one to two orders of magnitudes greater than these determined from the equivalent hydraulic apertures.

Fracture permeability under normal and shear stresses

The difference between the permeability under residual shear stress and that under peak stress becomes larger under higher normal stresses. The fracture hydraulic conductivities exponentially decrease with increasing the normal stresses. Their permeability is in the range between 1.0×10^{-3} m/s and 15×10^{-3} m/s. The fracture hydraulic conductivity determined here compares well with those obtained by Zhao J. (1998) and Chandra et al. (2008).

The flow in fractures is sensitive to normal stiffness of discontinuity. The normal stiffness however tends to increase with increasing stress. In this research, the range of normal stiffness is approximately from 1 to 18 GPa/m which is of the same order of magnitude with those obtained by Pyrak-Nolte et al. (2000).

ACKNOWLEDGTMENT

REFERENCES

ASTM D5607-95, Standard test method for performing laboratory direct shear strength test of rock specimens under constant normal force. *Annual Book of ASTM Standards*, 04.08, American Society for Testing and Materials, Philadelphia.

Bandis, S.C., Lumsden, A.C., and Barton, N.R. (1983). Fundamentals of Rock Joint Deformation. *International Journal of Rock Mechanics and Mining Sciences & Geomechanics Abstracts*. 20(6):249-268.

Barton, N. (1973). *Review of a New Shear-Strength Criterion for Rock Joints. Engineering Geology*. 7(4):287-332.

Chandra, S., Ahmed, S., Ram, A. and Dewandel, B. (2008). Estimation of hard rock aquifers hydraulic conductivity from geoelectrical measurements : A theoretical development with field application. *Journal of Hydrology*. 357(3-4) : 218-227.

Indraratna, B., and Ranjith, P. (2001). Hydromechanical Aspects and Unsaturated Flow in Joints Rock. Lisse : A. A. Balkema.

Lee, H.S. and Cho, T.F. (2002). Hydraulic characteristics of rough fractures in linear flow under normal and shear load. *Rock Mechanics and Rock Engineering*. Springer-Verlag Wien. 35(4):299-318.

Maini, Y.N.T. (1971). In situ hydraulic parameters in jointed rock-their measurement and interpretation. Ph.D. Thesis. Imperial College, London. 321 p.

Pyrak-Noltea, L.J. and Morrisa, J.P. (2000). Single fractures under normal stress: The relation between fracture specific stiffness and fluid flow. *International Journal of Rock Mechanics and Mining Sciences*. 37(1):245-262.

Suanprom, P. Obcheoy, J. and Fuenkajorn, K. (2009). Permeability of Rock Fractures under Shear Stresses. *EIT-JSCE Joint International Symposium Geotechnical Infrastructure Asset Management,* Bangkok, Thailand

Son, B.K., Lee, Y.K. and Lee, C.I. (2004). Elasto-plastic simulation of a direct shear test on rough rock joints. *International Journal of Rock Mechanics & Mining Sciences*. 41(3):1-6.

Zeigler, B. 1976. *Theory of Modelling and Simulation.* New York: John Wiley and Sons.

BIOGRAPHY

Miss. Jiranut Obcheoy was born on September 17, 1986 in Ratchaburi province, Thailand. She received his Bachelor's Degree in Engineering (Geotechnology) from Suranaree University of Technology in 2008. For her post-graduate, she continued to study with a Master's degree in the Geological Engineering Program, Institute of Engineering, Suranaree university of Technology. During graduation, 2008-2010, she was a part time worker in position of research assistant at the Geomechanics Research Unit, Institute of Engineering, Suranaree University of Technology. She published technical paper related to rock mechanics, titled **"Fracture Permeability under Normal and Shear Stresses"** in the Proceedings of the Third Thailand Symposium on Rock Mechanics, Petchaburi, Thailand.